



UNIVERSITY OF LEEDS

This is a repository copy of *Synthesis and characterization of C₂-symmetric bis(carboxamide) pincer ligands*.

White Rose Research Online URL for this paper:

<https://eprints.whiterose.ac.uk/208745/>

Version: Accepted Version

Article:

Razuwika, R. orcid.org/0000-0001-9831-7759 and Munro, O.Q. orcid.org/0000-0001-8979-6321 (2024) *Synthesis and characterization of C₂-symmetric bis(carboxamide) pincer ligands*. *New Journal of Chemistry*. ISSN 1144-0546

<https://doi.org/10.1039/d3nj05502g>

© The Royal Society of Chemistry and the Centre National de la Recherche Scientifique 2024. This is an author produced version of an article published in *New Journal of Chemistry*. Uploaded in accordance with the publisher's self-archiving policy.

Reuse

Items deposited in White Rose Research Online are protected by copyright, with all rights reserved unless indicated otherwise. They may be downloaded and/or printed for private study, or other acts as permitted by national copyright laws. The publisher or other rights holders may allow further reproduction and re-use of the full text version. This is indicated by the licence information on the White Rose Research Online record for the item.

Takedown

If you consider content in White Rose Research Online to be in breach of UK law, please notify us by emailing eprints@whiterose.ac.uk including the URL of the record and the reason for the withdrawal request.



eprints@whiterose.ac.uk
<https://eprints.whiterose.ac.uk/>

Synthesis and Characterization of C_2 -Symmetric Bis(Carboxamide) Pincer Ligands

Rufaro Razuwika^{*,a} and Orde Q. Munro^{a,b}

Received 00th January 20xx,
Accepted 00th January 20xx

DOI: 10.1039/x0xx00000x

Tridentate bis(carboxamide) pincers are key ligands used in catalysis, investigational medicinal inorganic compounds, and materials science. This study examined the atropisomerism of a group of bis(carboxamide) pincers with C_2 symmetry to elucidate their physical, chemical, and structural behaviour, paving the way for the application of their metal complexes in different fields. One of the five compounds structurally elucidated by X-ray crystallography, **1c**, has a pair of intramolecularly constrained isoquinoline ring substituents and crystallized enantiomerically pure in a chiral Sohncke space group. PM6 calculations of the 3-D potential energy surface for the main atropisomerisation reaction coordinate of **1c** indicated that the lowest-energy conformer (atropisomer) has the isoquinoline rings canted out-of-plane by almost $+30^\circ$ and -30° relative to the central pyridine ring. The X-ray structure of **1c** is located close to this energy minimum. Circular dichroism (CD) spectroscopy on bulk solid samples confirmed the presence of an excess population of one enantiomer (C_2 -symmetric atropisomer), most notably for compounds **1c**, **1e**, and **1f**. CD spectra could be recorded for all compounds in solution, similarly reflecting an excess population of one atropisomer. The experimental spectra were confirmed by TD-DFT simulations at the CAM-B3LYP/def2-tzvp level of theory. We conclude that the present group of ligands are worthy of further investigation as chelating agents for metal ions with applications in chiral catalysis or biology.

Introduction

Pincer molecules have been widely studied across the natural sciences due to their high thermal stability^{1,2} and ability to sterically control the metal centres to which they are bound as tridentate ligands in metal chelates.^{3,4} Some pincer molecules can selectively extract metal ions from the solution, which makes them important in separation and detection technologies.^{5,6} Although pincers are mainly used as chelating agents, several of them display additional functionality by complexing anions.^{7,8} Moreover, pincer-type receptors have been studied as potential ion channels in membranes due to their cation/anion-binding cores and their ability to form π -stacked arrays.^{6,9}

Pincer compounds can be asymmetrical or symmetrical. Symmetric pincer ligands generally have three main structural features: a central anchoring site (backbone), two equivalent "arms" which can form an achiral or chiral pocket (depending on their structure), and the metal binding site which is usually the tridentate chelating motif forming a functional cavity at the centre of the molecule. These structural attributes play an important role in metal complexes, especially in C_2 -symmetric catalysts capable of chiral induction,^{10,11} and these pincers are

capable of functioning as anion receptors.¹² For the most part, the core of a pincer molecule is planar. However, the size and orientation of the groups constituting the arms will dictate the global conformation as well as the physical and chemical properties of the molecule. Consequently, pincer compounds may be designed to function in particular ways.

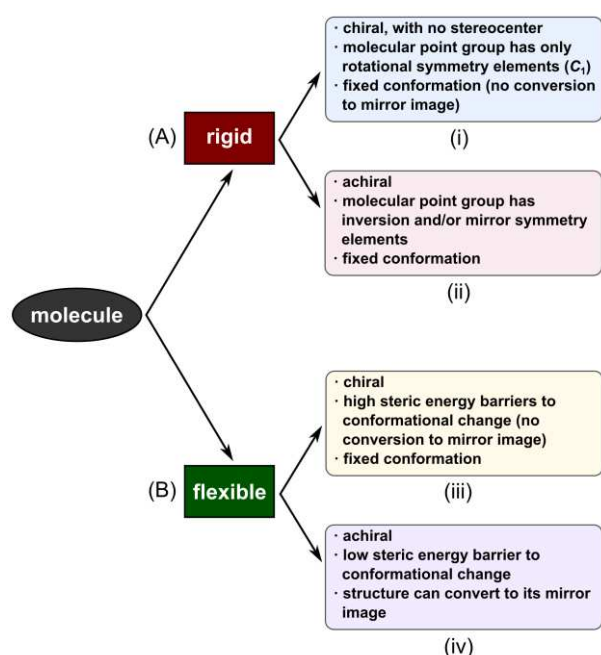
Even though many pincer molecules do not have stereogenic centres, flexibility and steric effects involving the pincer arms may introduce axial chirality (helicity) in the nominally planar molecule, producing atropisomers.^{10,11} The helicity in pincer molecules arises from the presence of a 2-fold rotation axis in the molecule, favouring crystallisation in space groups containing 2-fold and 2-fold screw axes.¹³ These compounds are therefore classified as P if they display right-handed helicity or exhibit a negative CD spectrum; the opposite is true for M isomers. Familiar examples of non-pincer atropisomers which possess C_2 symmetry and such chirality include the bidentate ligand BINAP (2,2'-bis(diphenylphosphino)-1,1'-binaphthyl)¹⁴ and ortho-condensed polycyclic aromatic compounds (i.e., helicenes).^{15,16}

Atropisomers arise due to the constrained rotation about a single bond due to steric strain; the influence of the steric strain on rotation allows for the isolation of various conformers.^{14,17} Notably, atropisomerism is a significant phenomenon in medicinal chemistry and plays an important role in pharmaceutical design,^{17–19} the behaviour of several natural products (e.g., Gossypol),²⁰ and the development of catalysts capable of asymmetric induction—specifically chirality-inducing ligands (e.g., BINOL and BINAP).²¹

^a Molecular Sciences Institute, School of Chemistry, University of the Witwatersrand, PO WITS 2050, Johannesburg, South Africa. Email: razuwika@gmail.com

^b School of Chemistry University of Leeds, Woodhouse Lane, LS2 9JT, UK. Email: O.Munro@leeds.ac.uk

Electronic Supplementary Information (ESI) available: X-ray crystal structures in CIF format (CCDC 2310781–2310785). See DOI: 10.1039/x0xx00000x



Scheme 1. An outline depicting the four scenarios, which allow molecules to crystallise in the 65 Sohncke space groups, i.e., those containing only symmetry operations of the first kind (rotations, rototranslations, translations).¹³

Scheme 1 outlines how molecules with no stereocentres crystallise in Sohncke space groups. The molecules can be rigid (A), locking them in one conformer, or flexible (B), which allows them to interchange between conformers. Pincer molecules are usually flexible as rotations are typically feasible about specific torsion angles (i.e., there are several internal degrees of freedom). Facile conversion to a mirror image conformer is typically allowed if the barrier to rotation of spatially separate groups (i.e., the pincer arms) in the molecule is low, as listed in scenario (iv) of Scheme 1. This usually requires that intramolecular nonbonded interactions remain above a distance threshold limit of *ca.* 1.5 Å for such rotations.²² Scenario (iii) prevails when this threshold cannot be met, and the molecule becomes locked in one conformation. Scenario (iii) results in spontaneous resolution, and the compound crystallises in only one conformer; the crystal structure then falls under a chiral Sohncke space group, usually $P2_12_12_1$.²² This phenomenon is absent in scenario (iv), so the compound crystallizes as a racemate, and its crystals will belong to an achiral Sohncke space group.²²

Bis(carboxamide) pincer molecules are a class of pincer molecules that have two amide groups connecting the substituent arms to the pincer core and typically display enhanced stability attributable to the presence of the amide bond.^{23–25} Delocalization of electrons involving the amide nitrogen lone pairs and adjacent aromatic rings further enhances the compounds' stability. Bis(carboxamide) pincers have been widely studied as their metal complexes but rarely as individual molecules.²⁶ Their stability at elevated temperatures and under a range of physical and chemical conditions,^{3,4,25,27} coupled with their potential chirality, suggests that metal-free

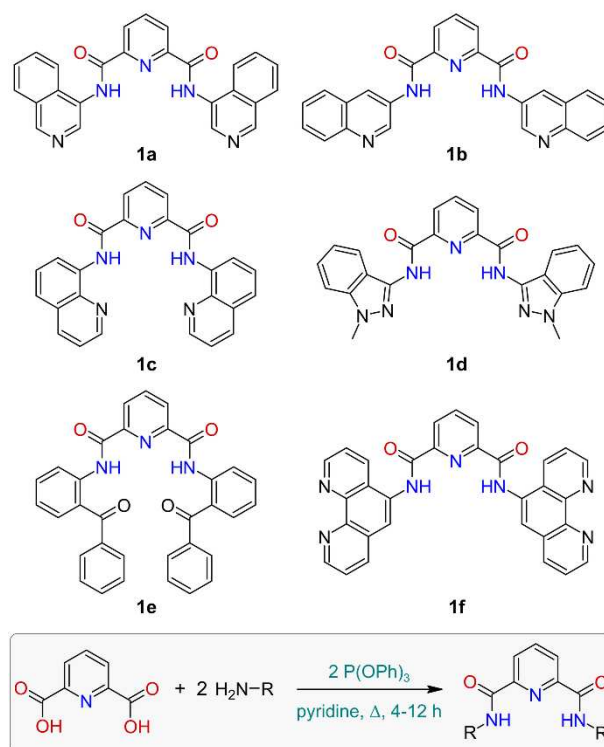


Figure 1: Structures and general synthetic scheme for bis(carboxamide) pincer compounds containing a central pyridine core and substituents capable of engendering C_2 symmetry for the molecule. Compound **1c** crystallised in the Sohncke space group $P2_12_12_1$; compounds **1b**, **1d**, and **1e** crystallised in non-Sohncke space groups.

bis(carboxamide) pincers might find applications in catalysis,^{4,28–31} luminescent material,^{32–35} molecular sensors,^{36–38} drug-design,³⁹ ion transport,^{40,41} and extraction metallurgy.^{5,42,43}

In this paper, we report on the synthesis, characterisation, and electronic and physical structures of several new and broadly related bis(carboxamide) pincer compounds (Figure 1) with intrinsic C_2 symmetry (gas and solution phase) as a foundation for exploring their future as C_2 -symmetry ligands for catalysis (notably chiral induction) or other applications.

Experimental

General

Pyridine-2,6-dicarboxylic acid, triphenyl phosphite and all amines were acquired from Sigma-Aldrich, except for 3-amino-1-methyl-1H-indazole, which was purchased from abcr GmbH. All solvents used for synthesis and spectroscopy (NMR and HRMS) were purchased from Sigma-Aldrich and generally used without further purification, except for acetonitrile and dichloromethane, which were dried over 5 Å molecular sieves. Spectroscopic grade solvents from Acros Organics were used for UV-vis spectroscopy without further purification.

Instruments

A Bruker Alpha II FTIR spectrometer with a Platinum ATR diamond sampling accessory was used to record FTIR spectra of crystalline solids. ^1H and ^{13}C NMR spectra were recorded on either a 300 MHz or 400 MHz Bruker Avance III NMR spectrometer fitted with auto-sampler accessories. The compounds were dissolved in deuterated solvents (chloroform- d_1 , dimethyl sulfoxide- d_6 (DMSO), acetonitrile- d_3 (ACN), methanol- d_3 , or N,N dimethylformamide- d_7 (DMF)). Standard Bruker pulse programs (298 K) were used, and chemical shifts were reported in δ (ppm) relative to the deuterated solvent signal. ^1H chemical shifts were referenced at 7.26, 2.50, 2.11, 4.87 and 2.92 ppm for CDCl_3 , $(\text{CD}_3)_2\text{SO}$, CD_3CN , CD_3OD , and $(\text{CD}_3)_2\text{NOCD}$, respectively, whereas δ ^{13}C was referenced at 77.16, 39.52, 118.26, 49.00 and 163.15 ppm, respectively.

Samples of pure compounds (typically *ca.* 10 $\mu\text{g}/\text{mL}$) were prepared in acetonitrile or ethanol for metal chelates and HPLC-grade methanol for ligands. Solutions were acidified using 0.1% (v/v) formic acid to obtain spectra in ESI+ mode. HRMS were recorded on a Bruker Compact Q-TOF high-resolution mass spectrometer by direct infusion at a flow rate of 5 $\mu\text{L}/\text{min}$ for 1 min (controlled by the system's Bruker Daltonics HyStar 3.2 SR4 software package). Samples were prepared in HPLC-grade methanol or acetonitrile (5% DMSO) (~ 10 $\mu\text{g}/\text{mL}$). Chromatograms were analysed with Bruker Compass Data Analysis software (Version 4.3). Melting points were determined visually on a hot-stage microscope instrument from JM-Inst. UV-vis (electronic) spectra were recorded on a single-beam Agilent 8453 spectrophotometer or a Specord 210[®] Plus double-beam spectrometer (Analytik-Jena) using WinASPECT Plus version 4.2.0.0. Cell holders were thermostatted at 25 $^\circ\text{C}$ using an external water circulator; 1.0 cm pathlength quartz cuvettes and spectroscopic grade DMSO or acetonitrile were used for all measurements. Circular dichroism (CD) spectra were recorded on a JASCO J-1500 MCD spectrometer in 1.0 cm pathlength quartz cuvettes using spectroscopic grade chloroform, methanol, or tetrahydrofuran (THF) as solvents. CD spectra of solid samples were recorded in diffuse reflectance mode using an integrating sphere and powdered compounds compressed into a 1.0-cm diameter sample holder.

X-ray diffraction intensity data were recorded on a Bruker Apex II 3-circle X-ray diffractometer or a Bruker D8 Venture 4-circle X-ray diffractometer at 153(1) or 173(1) K (Oxford CryoStream) using Mo $\text{K}\alpha$ radiation. Crystals were mounted in Paratone[®] oil using nylon micro-loops (Hampton) or polymer microgrippers (MiTeGen) for data collection. Using Olex2 1.5,⁴⁴ the structures were solved with the ShelXT⁴⁵ structure solution program (intrinsic phasing) and then refined using least squares minimisation to a good model (anisotropic atoms for all non-H atoms) with the ShelXL⁴⁶ refinement package. Each structure was further refined with Olex2 1.5 before implementing the final refinement cycles using non-spherical atom form factors (NSAFF) with NoSpherA⁴⁷ running in Olex2. The NSAFF were calculated from the electron density derived from a single determinant SCF wavefunction at the $r^2\text{SCAN}^{48}/\text{cc-pVTZ}^{49}$ level

of theory for a fragment of the crystal using Orca 5.0.4⁵⁰ for the density functional theory (DFT) calculations.

Synthetic procedures and X-ray crystallography data

All synthesised compounds were novel except for **1c**, N^2,N^6 -di(quinolin-8-yl)pyridine-2,6-dicarboxamide, which has been synthesised by Hiratani and Kaguchi.⁵ A method by Barnes *et al.*, was adapted and used for the synthesis of compounds **1a–1f** in this study.⁵¹ Generally, 2,6-pyridine dicarboxylic acid (1 eq) and the appropriate amine (2.1 eq) were heated under solvent reflux for several hours in the presence of triphenyl phosphite (2 eq) with pyridine as the solvent. The products were then precipitated from the solution by adding ethanol or hexane to the cooled reaction mixtures. Specific details are given below.

N2,N6-di(isoquinolin-4-yl)pyridine-2,6-dicarboxamide

(1a). 2,6-Pyridine dicarboxylic acid (1.5 mmol, 0.25 g) and 4-amino isoquinoline (3.2 mmol, 0.46 g) were stirred in 15 mL pyridine for 10 minutes at room temperature before adding triphenyl phosphite (3.0 mmol, 0.77 mL) and heating the reaction mixture under reflux for 4 h. After cooling the solution, ethanol was added to the reaction mixture, which was then left to stand on ice until a precipitate formed. The white precipitate was filtered off (Hirsch funnel) and washed with cold ethanol before being allowed to air-dry. Yield: 0.61 g, 97%. Single crystals were grown by slow diffusion of acetonitrile into a solution of the compound dissolved in DMSO. ^1H NMR (400 MHz, DMSO- d_6 , 298 K) δ 11.43 (s, 2H), 9.32 (s, 2H), 8.71 (s, 2H), 8.48(d, $J = 7.7$ Hz, 2H), 8.38 (dd, $J = 8.4, 7.1$ Hz, 1H), 8.23 (d, $J = 8.2$ Hz, 2H), 8.11 (d, $J = 8.4$ Hz, 2H), 7.89 (ddd, $J = 8.3, 6.8, 1.3$ Hz, 2H), 7.77 (t, $J = 7.5$ Hz, 2H). ^{13}C NMR (101 MHz, DMSO- d_6) δ 163.14, 151.14, 148.56, 141.11, 140.39, 132.13, 130.99, 128.68, 128.33, 128.02, 125.72, 122.76 HRMS (ESI+): m/z 420.1457 (calculated m/z for $\text{C}_{25}\text{H}_{17}\text{N}_5\text{O}_2$, $[\text{M}+\text{H}]^+$ 420.1455). UV-vis [DMSO; λ_{max} , nm ($10^3 \epsilon$, $\text{M}^{-1} \text{cm}^{-1}$): 277 (10.9), 309 (9.2), 323 (10.5). FTIR (powder, cm^{-1}): 1677.07 (C=O), 3283.13 (N–H), 3372.95 (N–H). Melting temperature: 400–410 $^\circ\text{C}$.

Crystal data for 1a: $\text{C}_{25}\text{H}_{17}\text{N}_5\text{O}_2$ ($M = 419.446$ g mol^{-1}): monoclinic, space group $P2_1/c$ (no. 14), $a = 8.7392(4)$ \AA , $b = 14.6766(8)$ \AA , $c = 15.2758(8)$ \AA , $\beta = 102.656(2)^\circ$, $V = 1911.70(17)$ \AA^3 , $Z = 4$, $T = 173.15$ K, $\mu(\text{Mo K}\alpha) = 0.096$ mm^{-1} , $D_{\text{calc}} = 1.457$ g cm^{-3} , 38141 reflections measured ($6.14^\circ \leq 2\theta \leq 66.46^\circ$), 7297 unique ($R_{\text{int}} = 0.0277$, $R_\sigma = 0.0189$) which were used in all calculations. The final R_1 was 0.0187 ($I \geq 2\sigma(I)$) and wR_2 was 0.0410 (all data).

N2,N6-di(quinolin-3-yl)pyridine-2,6-dicarboxamide (1b).

The same procedure described for **1a** above was used with 3-aminoquinoline (3.2 mmol, 0.46 g) in place of 4-aminoisoquinoline, and 2,6-pyridine dicarboxylic acid (1.5 mmol, 0.25 g). A yellow crystalline powder was produced after filtering off the precipitate and air-drying. Yield: 0.59 g, 94%. Single crystals were grown by slow evaporation from a solution of **1b** in methanol. ^1H NMR (400 MHz, DMSO- d_6 , 298 K) δ 11.41 (s, 2H), 9.35 (d, $J = 2.5$ Hz, 2H), 8.95 (d, $J = 2.5$ Hz, 2H), 8.43 (d, $J = 7.7$ Hz, 2H), 8.33 (dd, $J = 8.3, 7.1$ Hz, 1H), 8.01 (dt, $J = 8.3, 1.5$ Hz, 4H), 7.69 (ddd, $J = 8.5, 6.8, 1.4$ Hz, 2H), 7.60 (ddd, $J = 8.1, 6.8, 1.3$ Hz, 2H). ^{13}C NMR (101 MHz, DMSO- d_6 , 298 K) 162.34, 148.37, 145.88, 144.53, 140.30, 131.79, 128.52, 127.93, 127.70,

127.26, 125.66, 124.59. HRMS (ESI+): m/z 420.1455 (calculated m/z for $C_{25}H_{17}N_5O_2$, $[M+H]^+$ 420.1455), UV-vis [DMSO; λ_{max} , nm ($10^3 \epsilon$, $M^{-1} cm^{-1}$): 275 (23.6), 312 (17.5), 324 (17.7), 338 (15.9). FTIR (powder, cm^{-1}): 1682.70 (C=O), 3191.12 (N–H), 3063.25 (N–H). Melting temperature: 370–377 °C.

Crystal data for 1b: $C_{27}H_{25}N_5O_4$ ($M = 483.531 g mol^{-1}$): triclinic, space group $P-1$ (no. 2), $a = 7.2743(3) \text{ \AA}$, $b = 11.3528(5) \text{ \AA}$, $c = 14.9566(5) \text{ \AA}$, $\alpha = 76.605(1)^\circ$, $\beta = 78.871(1)^\circ$, $\gamma = 78.901(2)^\circ$, $V = 1164.76(8) \text{ \AA}^3$, $Z = 2$, $T = 153.00 \text{ K}$, $\mu(Mo K\alpha) = 0.095 \text{ mm}^{-1}$, $D_{calc} = 1.379 \text{ g cm}^{-3}$, 85728 reflections measured ($5.78^\circ \leq 2\theta \leq 66.42^\circ$), 8894 unique ($R_{int} = 0.0459$, $R_\sigma = 0.0265$) which were used in all calculations. The final R_1 was 0.0290 ($I \geq 2\sigma(I)$) and wR_2 was 0.0453 (all data).

N2,N6-di(quinolin-8-yl)pyridine-2,6-dicarboxamide (1c). The same procedure described for **1a** above was used with 8-aminoquinoline (3.2 mmol, 0.46 g) in place of 4-aminoisoquinoline, and 2,6-pyridine dicarboxylic acid (1.5 mmol, 0.25 g). A pale-yellow flaky powder was filtered off and dried. Yield: 0.62 g, 98%. Single crystals were grown by slow evaporation from a solution of **1c** in chloroform. 1H NMR (500 MHz, chloroform- d , 298 K) δ 12.36 (s, 2H), 9.03 (dd, $J = 7.3, 1.5 \text{ Hz}$, 2H), 8.59 (d, $J = 7.7 \text{ Hz}$, 2H), 8.27 (dd, $J = 4.2, 1.6 \text{ Hz}$, 2H), 8.20 (dd, $J = 8.1, 2.0 \text{ Hz}$, 3H), 7.70 – 7.61 (m, 4H), 7.33 (dd, $J = 8.2, 4.1 \text{ Hz}$, 2H). ^{13}C NMR (126 MHz, chloroform- d , 298 K) δ 162.02, 149.14, 148.79, 139.63, 139.33, 136.14, 134.45, 128.08, 127.38, 125.44, 122.35, 121.42, 117.31. HRMS (ESI+): m/z 420.1462 (calculated m/z for $C_{25}H_{17}N_5O_2$, 420.1455), $[M+H]^+$. UV-vis [DMSO; λ_{max} , nm ($10^3 \epsilon$, $M^{-1} cm^{-1}$): 326 (86.0). FTIR (powder, cm^{-1}): 1677.70 (C=O), 3320.57 (N–H), 3266.48 (N–H). Melting temperature: 308–319 °C.

Crystal data for 1c: $C_{25}H_{17}N_5O_2$ ($M = 419.446 g mol^{-1}$): orthorhombic, space group $P2_12_12_1$ (no. 19), $a = 4.4778(2) \text{ \AA}$, $b = 16.9420(7) \text{ \AA}$, $c = 25.8329(10) \text{ \AA}$, $V = 1959.76(14) \text{ \AA}^3$, $Z = 4$, $T = 173.15 \text{ K}$, $\mu(Mo K\alpha) = 0.094 \text{ mm}^{-1}$, $D_{calc} = 1.422 \text{ g cm}^{-3}$, 30705 reflections measured ($5.76^\circ \leq 2\theta \leq 56.54^\circ$), 4830 unique ($R_{int} = 0.0305$, $R_\sigma = 0.0205$) which were used in all calculations. The final R_1 was 0.0172 ($I \geq 2\sigma(I)$) and wR_2 was 0.0292 (all data).

N2,N6-bis(1-methyl-1H-indazol-3-yl)pyridine-2,6-dicarboxamide (1d). Following the method for **1a** above, 3-amino-1-methyl-1H-indazole (3.2 mmol, 0.44 g) was reacted with 2,6-pyridine dicarboxylic acid (1.5 mmol, 0.25 g). After cooling the reaction mixture, hexane was added to the solution, and the reaction flask was left to stand on ice until a precipitate formed. The cream-coloured precipitate was filtered, washed with cold ethanol, and air-dried. Yield 0.59 mg, 93%. Single crystals were grown by slow evaporation of a solution of the compound dissolved in acetonitrile. 1H NMR (400 MHz, DMSO- d_6 , 298 K) δ 11.79 (d, $J = 2.6 \text{ Hz}$, 2H), 8.46 (d, $J = 7.7 \text{ Hz}$, 2H), 8.34 (dd, $J = 8.3, 7.2 \text{ Hz}$, 1H), 7.84 (dq, $J = 8.2, 1.1 \text{ Hz}$, 2H), 7.64 (d, $J = 8.5 \text{ Hz}$, 2H), 7.44 (ddd, $J = 8.3, 6.9, 1.1 \text{ Hz}$, 2H), 7.15 (ddd, $J = 7.9, 6.8, 0.8 \text{ Hz}$, 2H), 4.05 (s, 6H). ^{13}C NMR (400 MHz, DMSO- d_6 , 298 K) δ 162.31, 148.55, 140.86, 139.95, 138.24, 126.56, 125.49, 122.25, 119.89, 117.47, 109.77, 35.24. HRMS (ESI+): m/z 426.1674 (calculated m/z for $C_{23}H_{19}N_7O_2$, $[M+H]^+$ 426.1673). UV-vis [CH_3CN ; λ_{max} , nm ($10^3 \epsilon$, $M^{-1} cm^{-1}$): 199 (71.1), 222 (18.4), 285 (15.2). FTIR (powder, cm^{-1}): 1690.18 (C=O), 3309.89 (N–H). Melting temperature: 298–305 °C.

Crystal data for 1d: $C_{23}H_{19}N_7O_2$ ($M = 425.453 g mol^{-1}$): monoclinic, space group $P2/c$ (no. 13), $a = 10.4220(2) \text{ \AA}$, $b = 11.8014(3) \text{ \AA}$, $c = 8.6298(2) \text{ \AA}$, $\beta = 112.076(1)^\circ$, $V = 983.60(4) \text{ \AA}^3$, $Z = 2$, $T = 153.15 \text{ K}$, $\mu(Mo K\alpha) = 0.097 \text{ mm}^{-1}$, $D_{calc} = 1.437 \text{ g cm}^{-3}$, 23461 reflections measured ($4.22^\circ \leq 2\theta \leq 63.28^\circ$), 3318 unique ($R_{int} = 0.0294$, $R_\sigma = 0.0180$) which were used in all calculations. The final R_1 was 0.0259 ($I \geq 2\sigma(I)$) and wR_2 was 0.0639 (all data).

N2,N6-bis(2-benzoylphenyl)pyridine-2,6-dicarboxamide (1e). The method for **1a** above was applied with 2-amino benzophenone (3.2 mmol, 0.63 g) in place of 4-amino isoquinoline and 2,6-pyridine dicarboxylic acid (1.5 mmol, 0.25 g). After cooling the reaction mixture, ethanol was added to the solution and the reaction flask was left to stand on ice until a precipitate formed. The pale orange precipitate was filtered, washed with cold ethanol, and left to air-dry. Yield 0.75 mg, 95%. Single crystals were grown in a binary mixture of ethanol and water (50% v/v). 1H NMR (300 MHz, chloroform- d , 298 K) δ 12.32 (s, 2H), 8.54 (d, 2H), 8.35 (d, $J = 7.7 \text{ Hz}$, 2H), 8.04 (t, $J = 7.8 \text{ Hz}$, 1H), 7.69 – 7.57 (m, 8H), 7.49 (t, 2H), 7.31 (t, $J = 7.7 \text{ Hz}$, 4H), 7.28 – 7.22 (m, 2H). ^{13}C NMR (101 MHz, chloroform- d , 298 K) δ 191.86, 156.10, 142.77, 133.49, 132.52, 132.51, 127.47, 126.80, 126.47, 124.27, 122.21, 121.55, 119.33, 117.78, 117.06. HRMS (ESI+): m/z 526.1760 (calculated m/z for $C_{33}H_{23}N_3O_4$, $[M+H]^+$. 526.1761), UV-vis [DMSO; λ_{max} , nm ($10^3 \epsilon$, $M^{-1} cm^{-1}$): 333 (18.5), FTIR (powder, cm^{-1}): 1619.35 (C=O), 1550.12 (C=O), 3431.41 (N–H), 3311.14 (N–H). Melting temperature: 207–212 °C.

Crystal data for 1e: $C_{33}H_{23}N_3O_4$ ($M = 525.568 g mol^{-1}$): monoclinic, space group $P2_1/n$ (no. 14), $a = 8.4952(2) \text{ \AA}$, $b = 18.3345(4) \text{ \AA}$, $c = 16.2123(3) \text{ \AA}$, $\beta = 90.689(1)^\circ$, $V = 2524.97(9) \text{ \AA}^3$, $Z = 4$, $T = 153.15 \text{ K}$, $\mu(Mo K\alpha) = 0.092 \text{ mm}^{-1}$, $D_{calc} = 1.383 \text{ g cm}^{-3}$, 38759 reflections measured ($3.36^\circ \leq 2\theta \leq 56.76^\circ$), 6322 unique ($R_{int} = 0.0562$, $R_\sigma = 0.0479$) which were used in all calculations. The final R_1 was 0.0330 ($I \geq 2\sigma(I)$) and wR_2 was 0.0550 (all data).

N2,N6-di(1,10-phenanthrolin-5-yl)pyridine-2,6-dicarboxamide (1f). 1,10-phenanthrolin-5-amine (3.3 mmol, 0.66 g) was used in place of 4-amino isoquinoline with 2,6-pyridine dicarboxylic acid (1.5 mmol, 0.25 g), under the same reaction conditions described for **1a**. After cooling the reaction mixture, ethanol was added to the solution and the flask was left to stand on ice until a precipitate formed. The pale orange precipitate was isolated by gravity filtration, washed with cold ethanol, and left to air-dry. Yield 0.77 mg, 98%. 1H NMR (500 MHz, DMSO- d_6 , 298 K) δ 11.61 (s, 2H), 9.19 (dd, $J = 4.2, \text{ Hz}$, 2H), 9.12 (dd, $J = 4.3, 1.7 \text{ Hz}$, 2H), 8.69 (dd, $J = 8.3, 1.8 \text{ Hz}$, 2H), 8.59 (dd, $J = 8.1, 1.7 \text{ Hz}$, 1.6 Hz, 2H), 8.53 (d, $J = 7.7 \text{ Hz}$, 2H), 8.45 – 8.41 (m, 1), 8.27 (s, 2H), 7.91 (dd, $J = 8.3, 4.3 \text{ Hz}$, 2H), 7.82 (dd, $J = 8.1, 4.3 \text{ Hz}$, 2H). ^{13}C NMR (126 MHz, DMSO- d_6 , 298 K) 163.53, 150.69, 150.45, 148.98, 146.27, 144.80, 140.82, 136.72, 133.14, 131.83, 128.37, 126.34, 126.13, 124.24, 124.06, 123.70, 119.27. HRMS (ESI+): m/z $[M+H]^+$: 522.1773 (calculated m/z for $C_{31}H_{19}N_7O_2$, 522.5357), $[M+H]^+$. UV-vis [DMSO; λ_{max} , nm ($10^3 \epsilon$, $M^{-1} cm^{-1}$): 269 (75.0), 315 (15.6). FTIR (powder, cm^{-1}): 1658.67 (C=O), 3380.22 (N–H). Melting temperature: 270–279 °C.

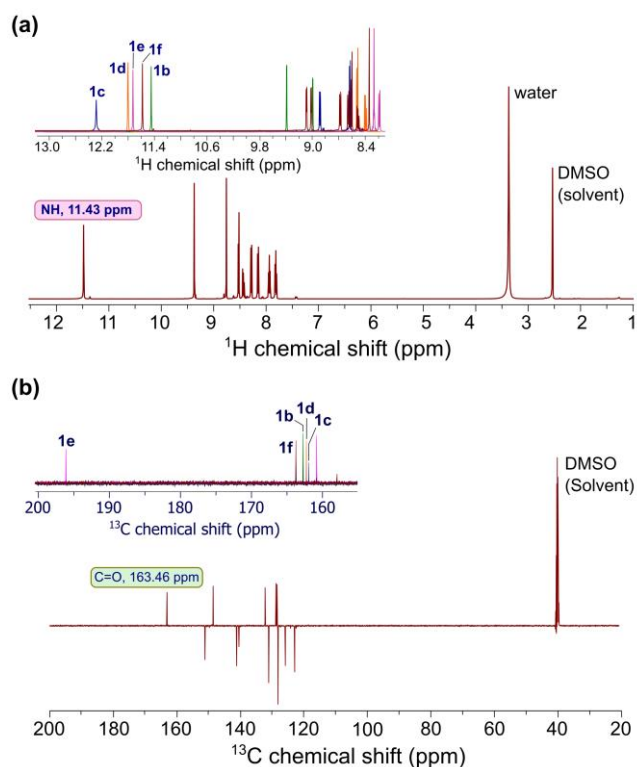


Figure 2. Illustration of the proton (a) and carbon (b) NMR spectra for **1a** (maroon lines, main spectra). The inset figures, in each case, display the variation in the chemical shift of the amide NH protons and the C=O carbons for the pincer compounds **1b–1f**.

Molecular simulations

DFT calculations were carried out with the multiprocessor version of Gaussian 16W⁵² interfaced to GaussView 6.1.1.⁵³ The X-ray structures of **1a–1e** were used as input geometries for the simulations after the removal of solvent molecules; the input structure of **1f** was built by editing and augmenting the structure of **1c**. The structures were initially geometry optimised *in vacuo* at the CAM-B3LYP⁵⁴/def2tzvp⁵⁵ level of theory; frequency calculations were used to simulate the compound's IR spectra and to establish the nature of all stationary points. All analysed minima were characterised by the absence of negative eigenvalues. TD-DFT⁵⁶ simulations (60 excited states) at the same level of theory were used to simulate the compound's electronic absorption and electronic circular dichroism (ECD) spectra. The electronic structures of the compounds were also simulated in a chloroform solvent continuum (PCM-SCRF method)⁵⁷ to evaluate the effect of a solvent on the spectroscopic properties of the compounds.

A full potential energy scan of conformational space for each compound was performed using the semi-empirical method PM6⁵⁸ both *in vacuo* and in a DMF solvent continuum to gauge the barrier to conformational inversion. The torsion angle scans were affected by driving ϕ_1 and ϕ_1' (see Figure 4b) asynchronously from 0–360° in 10° steps (Figure 6). The torsion angles ϕ_3 and ϕ_3' were treated similarly to give three-dimensional potential energy surfaces mapping the rotational energy dynamics of **1c**.

Table 1. Chemical shifts for specific protons and carbons from ¹H and ¹³C NMR and experimental melting temperature ranges for the synthesised pincer ligands

	Amide NH (ppm)	Amide C (ppm)	Melting Temperature range (°C)
1a	11.43	163.46	400-410
1b	11.45	162.82	370-377
1c	12.30	164.27	308-319
1d	11.80	161.85	298-305
1e	12.24	156.10	207-212
1f	11.62	163.54	270-279

Results and Discussion

General synthesis and characterisation

The carboxamide pincer compounds were synthesised by refluxing 2,6-pyridine dicarboxylic acid with the appropriate amine in pyridine in the presence of triphenyl phosphite, Figure 1. All reactions had high yields, in the 90–97% range. The synthesised products were fully characterised using ¹H, ¹³C and 2D NMR, FT-IR, mass spectroscopy, UV-vis spectroscopy, melting temperatures and X-ray crystallography. Computational studies on the compounds were also conducted to compare theoretical data to experimental data to further understand the compounds.

¹H, ¹³C and 2D NMR were primarily used to characterise the pincers. The main characteristic of the pincers is the amide proton, which is signalled by a single peak downfield in the spectrum, between 9 and 13 ppm, Table 1 and Figure 2. The chemical shifts of the amide proton are highly influenced by the arms of the pincer since they are the only variable in the molecules.

The pincer arms in **1a–1c** comprise different structural isomers of quinoline. There is enhanced deshielding of the amide protons due to the proximity of the quinoline nitrogen atoms to the amide proton 2–3 atoms away; hence the proton signals are found further downfield in the spectrum in comparison to the proton signals in **1e** and **1f**. Of the three quinolines, **1c** has the highest NH chemical shift, which is attributed to the proximity of the proton of interest to the adjacent molecule through space. The amide proton signal for **1d** falls within a similar range for the same reason, although the chemical shift is higher due to the presence of the indazole ring. The amide proton in **1d** has a higher chemical shift than the amide proton in **1e** because the benzophenone group on the arms of **1e** reduces the electron-donating capacity of the entire group when compared to the phenanthroline group in **1f**. The same principles apply to the chemical shifts of the amide carbons. The vast difference in the melting temperature ranges of the isomeric pincers (Table 1) is attributed to the structural differences in the pincer arms.

The reported melting temperatures of the pincers fall within the range of 207 °C to 410 °C (Table 1). These high melting temperatures demonstrate the enhanced stability of the compounds, which showed no decomposition at elevated temperatures (above 200 °C). This presumably reflects strong intermolecular interactions, like hydrogen bonding, which

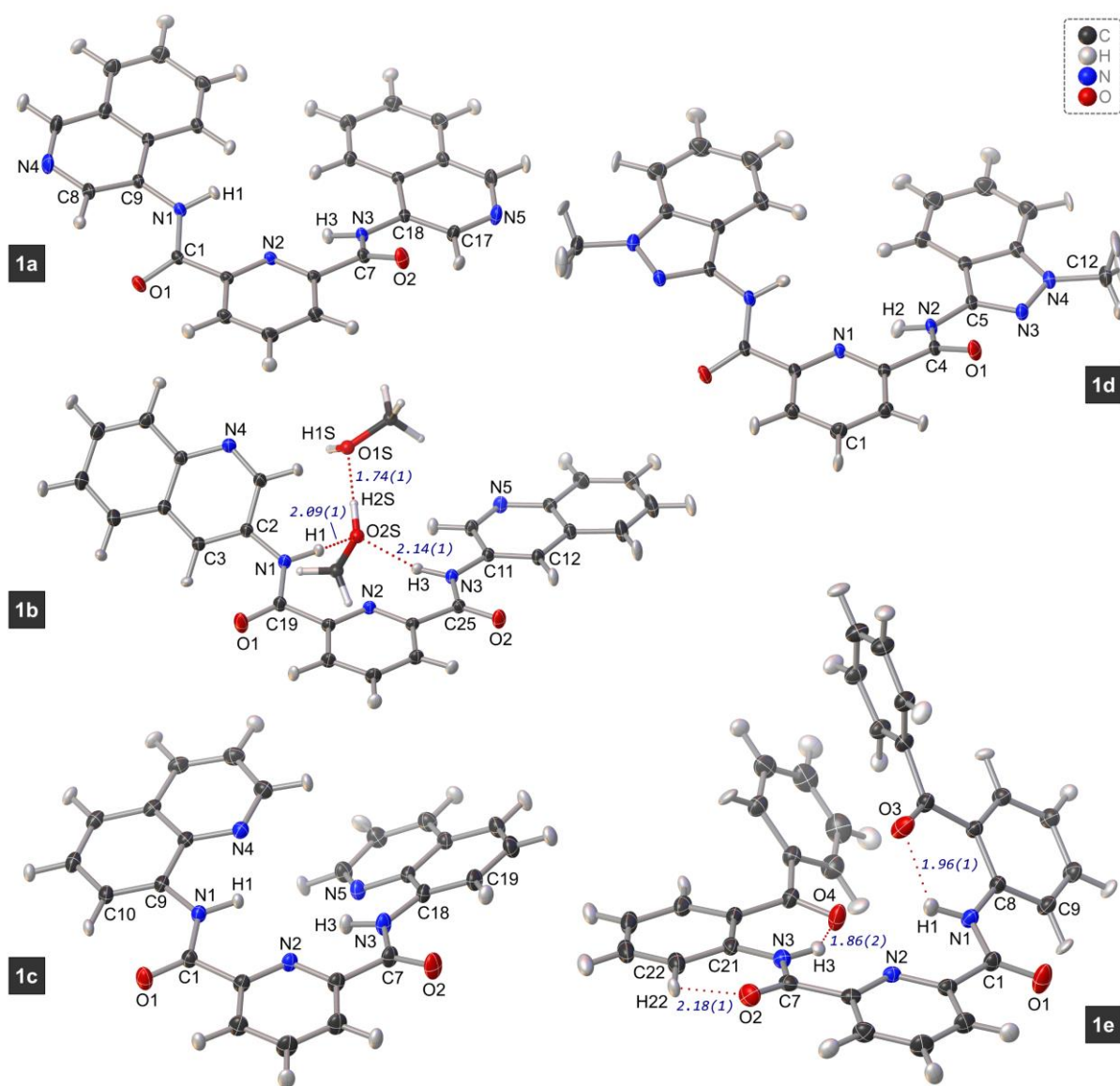


Figure 3. Selectively labelled views of the X-ray crystal structures of **1a–1e** refined with non-spherical atom form factors (NoSpherA2 within Olex2). Thermal ellipsoids are rendered at the 50% probability level (C, N, O). Hydrogen atom thermal ellipsoids are scaled to have the same equivalent isotropic displacement parameter, U_{eq} , as the attached heavy atom. H-bond distances and angles for **1b**: N5...H1S, 1.813(8) Å; H1...O2S, 2.086(6) Å; H3...O2S, 2.141(6) Å; H2S...O1S, 1.744(9) Å; N5...H1S...O1S, 168.3(7)°; N1...H1...O2S, 133.5(5)°; N3...H3...O2S, 158.8(5)°; O2S...H2S...O1S, 174.4(7)°. H-bond distances and angles for **1e**: H1...O3, 1.96(1) Å; H3...O4, 1.86(1) Å; H22...O2, 2.18(1) Å; N1...H1...O3, 126(1)°; N3...H3...O4, 137(1)°; C22...H22...O2, 120.6(7)°. Space groups: $P2_1/c$, **1a**; $P\bar{1}$, **1b**; $P2_12_12_1$, **1c**; $P2_1/c$, **1d**; $P2_1/n$, **1e**. Significant nonbonded crystal packing and hydrogen bonding interactions break the intrinsic C_2 symmetry of **1a**, **1b**, and **1e**, preventing their crystallisation in Sohncke space groups. Only **1d** has exact C_2 symmetry in the crystalline solid state; however, crystallisation as a C_i symmetry dimer restricts it to a regular space group. Compound **1c** has C_1 point group symmetry due to asymmetric packing interactions which break its C_2 symmetry. Since higher-symmetry oligomer formation is absent, **1c** is the only compound of the series that crystallises in a chiral space group.

requires more energy for melting relative to compounds bound by hydrophobic interactions and π -stacking. The extensiveness of π -stacking in compounds, however, significantly affects the strength of the intermolecular interactions; the aromatic nature of **1a–1f** likely enhances their stability further.

Figures 4(a), S25 and S26, illustrate the type of hydrogen bonding in each compound. Pincer **1a** has the highest melting point as it exhibits intermolecular hydrogen bonding, unlike the other pincers, which only exhibit intramolecular hydrogen bonding. The crystallographic data of **1b** did not provide enough information on the type of intermolecular interactions between the molecules, as methanol co-crystallised with the

compounds. It is, however, assumed that the high melting temperature resulted from strong intermolecular interactions in the compound. Pincer **1c**, which exhibits intramolecular hydrogen bonding, has the lowest melting temperature among the quinoline-based pincers, as the main forces of intermolecular interactions in the compound are π -stacking and hydrophobic interactions. Pincer **1d** is an anomaly to this trend as it has a significantly lower melting temperature than **1c** despite exhibiting inter-molecular hydrogen bonding. Pincer **1e** has the lowest melting point of all the pincers. The pincer arms of **1e** are flexible and do not allow for close packing, as there is additional distortion, which results in the arms losing their

planarity. All the other pincers, however, π -stack to different degrees. **1f** presumably exhibits the most π -stacking because of the three aromatic rings on each pincer arm, thus enhancing the interaction between its atoms.

X-ray crystallography

Single crystals suitable for X-ray diffraction were grown for **1a–1e** either by slow solvent diffusion or by slow evaporation. The diffraction data were collected at low temperature (≤ 173.15 K) to $2\theta > 56^\circ$, even for the weakest diffracting samples. The structures refined to impressively low R -factors (typically $\sim 2\%$ and ~ 5 – 9% better R_1 and wR_2 values, respectively) using non-spherical atom form factors (NoSpherA⁴⁷ implemented in Olex2⁴⁴) from electron density distributions calculated at the r^2 SCAN⁴⁸/cc-pVTZ⁴⁹ level of theory (DFT).

The low-temperature X-ray structures of the five pincer compounds are shown in Figure 3. All the compounds studied exhibit intrinsic C_2 symmetry (or C_{2v} symmetry in the case of **1d**) in the gas phase or solution (DFT simulations, *vide infra*), which hinges on each arm within the pincer having identical dihedral angles spanning the amide linker groups. Exact C_2 symmetry is mainly feasible for relatively rigid, isolated structures. However, the mean conformation of a statistical ensemble of symmetrically substituted flexible pincers containing a 2-fold axis of rotation in solution may also display C_2 point group symmetry if the planar C_{2v} structure is a transition state between inverted C_2 symmetry conformers and thus only transiently populated. In the crystalline solid state, significant nonbonded packing interactions, hydrogen-bonding, and dimer or oligomer formation are likely to induce local twisting of the lowest energy C_2 symmetry conformer or introduce an additional symmetry element such as a centre of inversion. Distortions in the compounds will destroy any intrinsic C_2 symmetry, while the formation of dimeric inversion pairs (C_i symmetry) through hydrogen bonding between C_2 symmetry monomers will preserve the intrinsic C_2 symmetry of each interacting moiety but ensure crystallisation in a non-Sohncke space group. Thus, the expectation is that flexible pincers with intrinsic C_2 symmetry will rarely crystallise with exact crystallographic C_2 symmetry in a Sohncke space group.

From the X-ray structures of **1a–1e** (Figure 3), only **1c** crystallises as a monomer in the chiral Sohncke space group $P2_12_12_1$; its conformation is, however, distorted by crystal packing interactions and thus lacks precise C_2 symmetry (despite this being possible in the gas phase). Although uncommon in the literature, pincers based on a pyridine core that crystallise in chiral space groups are known and typically exhibit C_1 point group symmetry due to deviations from ideal C_2 symmetry engendered by crystal packing forces. Three pertinent examples highlighting this general trend are N,N' -bis(2-methoxyphenyl)pyridine-2,6-dicarboxamide (CSD code CABWUY, space group $P2_12_12_1$),⁵⁹ tetra-*n*-butylammonium N,N' -bis(2,3-dimethyl-1*H*-inden-7-yl)-2,6-pyridinedicarboxamide fluoride (EDIKOS, $P2_1$),⁶⁰ and 2,6-dicarbonyl-bis(2'-amino-2''-*L*-methylalaninebenzanilidyl)pyridine (GICKEY, $P1$).⁶¹ The latter pincer compound contains enantiopure pincer arms and possesses helical symmetry, making it suitable as a

tridentate ligand for chiral induction in catalysis. Of the 250 bis(arylcarboxamide)pyridine pincers currently present in the Cambridge Structural Database (CSD),⁶² only 13 (or 5%) of the non-macrocyclic structures crystallise in chiral space groups ($P1$ and $P2_12_12_1$ being the most common). As might be expected, the structure of **1c** reported here at 173 K is broadly similar to that reported at 294 K (CSD code NIWNUD, $P2_12_12_1$);⁶³ the data quality is, however, superior.

Interestingly, pincers **1a** and **1d** form hydrogen-bonded dimers with C_i symmetry (i.e., inversion pairs) in the solid state, with the individual monomers making up each dimer exhibiting near (**1a**) or exact (**1d**) C_2 symmetry, Figure 4(a). These two structures are, therefore, achiral. Collectively, and considering the symmetry of the monomeric pincer ligands, only one of the five structures crystallised here (**1d**) displays crystallographic C_2 symmetry. The key questions are (i) How common are crystalline C_i symmetry dimers formed by bis(arylcarboxamide)pyridine pincers in the literature, and (ii) how many of these comprise monomers with exact C_2 symmetry? Inspection of the 250 structures available in the CSD for this class of compounds indicates that only 13 (or 5%) of the compounds comprise C_2 symmetry monomers within hydrogen-bonded or π -stacked inversion pairs (C_i symmetry dimers). Only one compound (N,N' -bis(2-((4-oxopent-2-en-2-yl)amino)phenyl)pyridine-2,6-dicarboxamide; CSD code POHNOQ)⁶⁴ crystallises in the space group $P2/c$ (akin to **1d**); the remaining 12 compounds crystallise in the related space group $C2/c$. Salient examples with similar structures to **1d** include N,N' -bis(4-bromophenyl)pyridine-2,6-dicarboxamide (CSD code MEWNEJ),⁶⁵ N,N' -bis(4-methyl phenyl)pyridine-2,6-dicarboxamide (CSD code RABZUQ),⁶⁶ and more elaborate helical C_2 symmetry derivatives such as N,N' -bis(2-(((anthracen-9-yl)methylidene)amino)phenyl)pyridine-2,6-dicarboxamide (CSD code WOMTOK).⁶⁷ The remaining structures in the series (**1b**, **1e**) have reduced molecular symmetry (C_1) due to conformational distortions engendered by nonbonded crystal packing interactions and/or hydrogen-bonding interactions. In the case of **1b**, hydrogen bonding to the solvent methanol molecules significantly distorts the conformation from ideal (expected) C_2 symmetry (Figure S25). For the above reasons, **1a**, **1b**, **1d**, and **1e** all crystallise in non-Sohncke space groups (they are flexible and belong to Group B (iv) in Scheme 1), despite their inherent propensity to adopt C_2 molecular symmetry in the gas phase (DFT simulations, *vide infra*).

Clearly, the key conformational signature of structures **1a–1e** is that none are planar; the substituent arms of the pincers are all canted relative to the mean plane of the pyridine core (Table 2, Figure 4(b)). For **1b**, the nonplanarity is particularly marked with the 10-atom mean plane of the quinoline ring containing N4 canted by 40.6° relative to the 8-atom mean plane of the central pyridine ring and the two carbonyl carbon atoms of the amide substituents. The distortion reflects the formation of a C–H \cdots N hydrogen bond between the quinoline ring's nitrogen atom (N4) and the *para*-C–H group of the neighbouring pincer's central pyridine ring (Figure S25). Nonbonded crystal packing interactions, which include hydrogen bonding to solvent methanol molecules, clearly

Table 2. Selected geometric and conformational data for the low temperature X-ray structures of **1a–1e**. Standard uncertainties (where relevant) for the least significant digit are given in parentheses.

Parameter	1a	1b	1c	1d	1e
C=O ave (Å)	1.227(1)	1.223(4)	1.223(3)	1.2282(7)	1.219(4), 1.228(1) ^c
(CO)–N ave (Å)	1.359(4)	1.356(3)	1.349(1)	1.3516(8)	1.356(5)
Δ_1 (°) ^a	10.6	40.6	9.0	1.6	37.9
Δ_2 (°) ^a	5.6	8.6	24.4	1.6	12.4
ϕ_1 (°) ^b	156.63(3)	169.32(5)	174.75(5)	154.67(6)	–166.29(9)
ϕ_1' (°) ^b	155.95(3)	177.14(5)	167.56(5)	154.67(6)	–169.98(9)
ϕ_2 (°) ^b	–175.34(3)	–171.33(5)	173.83(5)	178.50(5)	–179.8(1)
ϕ_2' (°) ^b	–175.89(3)	179.78(4)	178.69(6)	178.50(5)	172.9(1)
ϕ_3 (°) ^b	–159.67(3)	154.32(5)	–177.65(6)	–154.54(6)	–156.3(1)
ϕ_3' (°) ^b	–155.44(3)	175.55(5)	164.34(6)	–154.54(6)	174.7(1)

^a Δ_1 and Δ_2 are dihedral angles between the mean plane of the central pyridine ring and the mean plane of the pincer aryl group appended to the amide groups containing O1 and O2, respectively (see Figure 4b). ^b The three torsion angles spanning the amide groups containing carbonyl oxygen atoms O1 and O2 are labelled ϕ_1 – ϕ_3 and ϕ_1' – ϕ_3' , respectively (Figure 4b), and are measured (Figure 5) by default as their obtuse angles. The torsion angles ϕ_3 and ϕ_3' , for example, gauge the tilts of the aryl substituents (“arms”) relative to the pyridine ring core of the pincer. ^c Mean C–O bond distance for the two non-amide carbonyl groups.

perturb the conformation of **1b**, which would otherwise be flat and have exact C_{2v} symmetry (its ideal gas-phase geometry). For **1a** and **1d**, the nonplanarity observed in the crystalline solid state reflects (i) the conformational adjustment made by each monomer to establish a C_i symmetry dimer (inversion pair) and (ii) canting of the resultant closely juxtaposed isoquinoline or indazole rings to avert a significant intramolecular steric clash (Figure S26). For **1c**, the intramolecular steric repulsion between what would amount to being substantially overlapped quinoline rings in a planar conformation is acute, such that only a nonplanar conformer is feasible. However, from Table 2 and Figure 4 (b), the two quinoline rings are not canted equally relative to the plane of the central pyridine ring of the pincer, thereby obviating exact C_2 point group symmetry for the molecule. The conformational perturbation evident for **1c** mainly reflects sandwiching of the N4 quinoline ring between a pair of neighbouring molecules by C–H... π hydrogen bond formation (Figure S27).

As summarised in **Table 2**, the structures of **1a–1e** are all similar in terms of the geometry of their amide groups, with the average C=O and (CO)–N bond distances falling tightly in the ranges 1.22–1.23 Å and 1.35–1.36 Å, respectively, which are typical for metal-free amides.⁶⁸ This observation is consistent with negligible perturbation of the electron delocalisation over the amide groups, irrespective of the nature of the appended aryl rings or the conformational distortion induced by crystal packing. The latter effect on the amide groups can be seen in the parameter, ϕ_2 (or ϕ_2'), which deviates by $\sim 9^\circ$ at most from the ideal torsion angle of 180° in the case of **1b**. From Figure 5, the three torsion angles for **1a–1e** listed in Table 2 all fall within two standard deviations of the mean (180°) in each case and display the same pattern of variance with ϕ_1 and ϕ_3 evidently more flexible and prone to out-of-plane distortions than the central torsion angle of the amide group itself (ϕ_2). In the case of structures such as **1c**, and as noted above, intramolecular steric strain (repulsion between quinoline rings) is the main

driving force for the observed nonplanar conformation, especially since **1c** exhibits few other short nonbonded contacts in the crystal lattice.

The fundamental question is what happens to the conformation of each compound upon dissolution and solvation? Dissociation of any oligomers or dimers and the formation of a statistical ensemble of lowest-energy conformers dependent on the temperature and physical properties of the solvent would be expected. And only the most rigid conformers (those “locked in” by high steric energy barriers to inversion such as **1c**) might retain solution conformations like those observed in their crystal structures. The remainder of this paper attempts to delineate the solution behaviour of **1a–1f** to shed further light on key aspects of the conformational dynamics of this class of pincers.

Conformational analysis

X-ray crystallography and PM6 simulations. Single crystal X-ray data provides key atomic-resolution insights on the stereochemistry and conformation of each pincer in the crystalline phase. Our structural study reveals that the ostensibly planar pincers in fact have notably different conformations and that lattice packing effects may confer chirality on a pincer with appropriately sized and shaped substituents.^{5,60,61} This is supported by our analysis of the spread in the torsion angles of this class of pincers in the CSD (Figure 5) which reveals that distortions up to 30° from planarity are experimentally observed.

As mentioned earlier, **1c** crystallised in a chiral space group, indicating chirality in the pincer compound. Upon further analysis, it was concluded that all the compounds may exhibit axial chirality due to the presence of a crystallographic 2-fold screw axis or molecular C_2 axis passing through the molecules and should thus exist as atropisomers (Figure 3). The atropisomer enantiomer which crystallizes in the case of **1c** exhibited left-handed helicity and can be assigned as the M

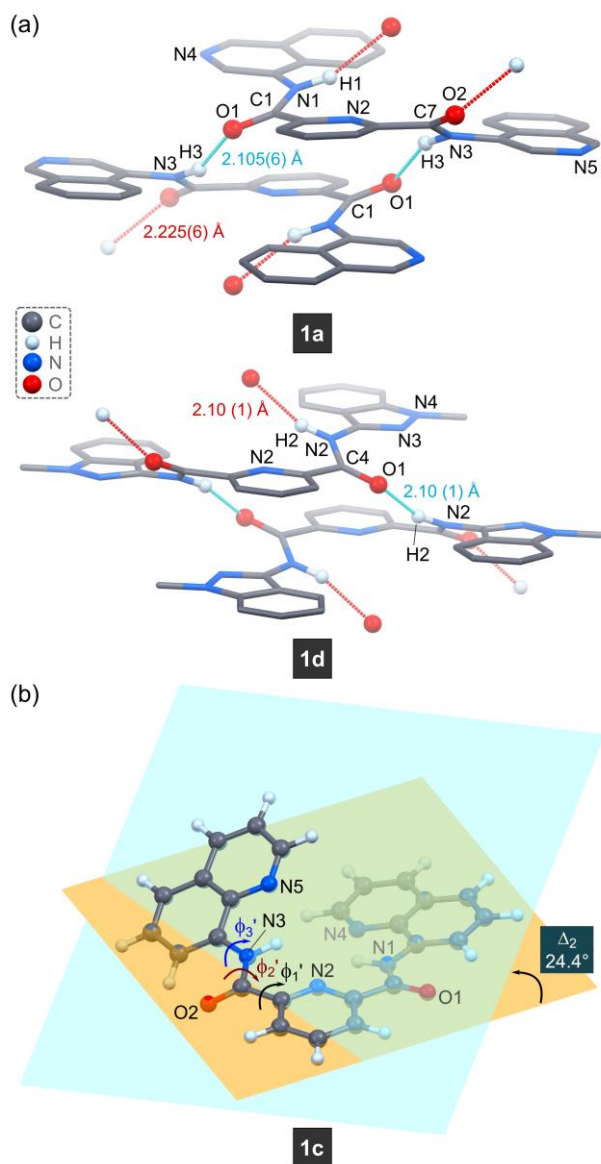


Figure 4. (a) View of the C_i symmetry hydrogen-bonded dimers formed by monomers of **1a** (top; symmetry codes x,y,z and $1-x,1-y,1-z$) and **1d** (bottom, exact C_2 point group symmetry; symmetry codes x,y,z and $1-x,y,1/2-z$). The linear chain of dimers (**1a**) or evenly spaced monomers (**1d**), where assembly is about centres of inversion in the lattice, favours crystallisation in non-Sohncke space groups. Non-polar hydrogen atoms are omitted for clarity; atoms involved in hydrogen bonding are rendered as spheres (arbitrary radii). (b) Illustration highlighting the nonplanarity of pincer **1c** and the dihedral angle (Δ_2 , 24.4°) between the planes passing through the central pyridine ring and the canted quinoline ring appended to the amide group containing carbonyl oxygen O2. Torsion angles defining the orientation of the second quinoline ring substituent (ϕ_1' – ϕ_3') are defined; the equivalent torsion angles for the first quinoline ring (right side) are ϕ_1 – ϕ_3 (i.e., unprimed).

(minus) stereoisomer. The M-helicity assignment was unambiguously confirmed by the negative CD bands⁶⁹ appearing in the CD spectra of solid **1c** (Figure 9).

The conformational energy landscape of **1c** was calculated by semi-empirical quantum mechanics (gas phase, Figure 6) and provides the appropriate 2-D and 3-D energy mapping to reveal that the X-ray structure is very close to the global minimum (a mildly nonplanar structure with $\phi_1 = \phi_1' \cong 180^\circ - 30^\circ = 150^\circ$), despite being potentially subject to crystal packing effects.

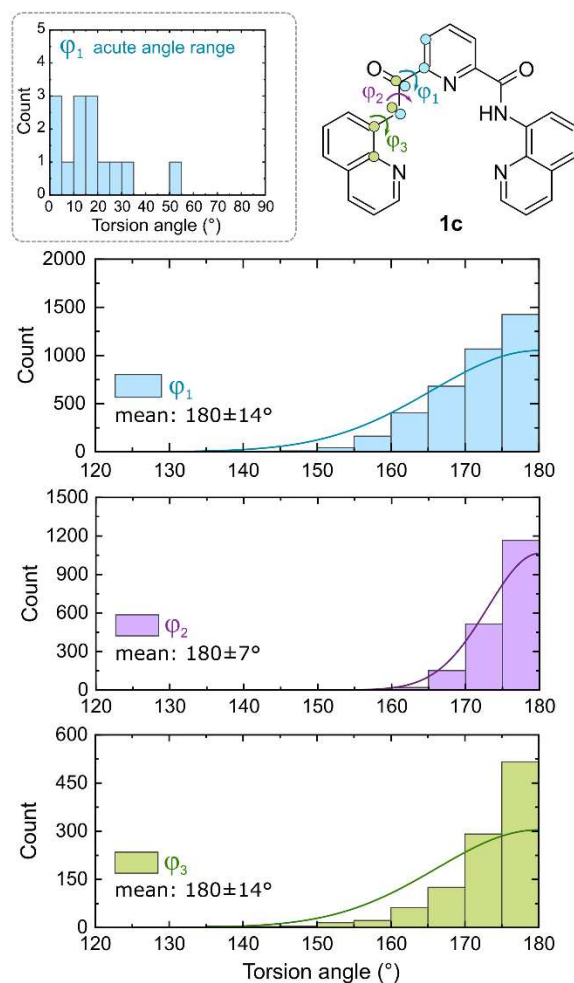


Figure 5. Histograms displaying the distribution of the torsion angles ϕ_1 – ϕ_3 from an analysis of all available X-ray structures with the same functional group components as **1c** in the CSD. For ϕ_2 and ϕ_3 there are < 6 structures in each case with the torsion angle < 90° in contrast to ϕ_1 which, though still rare (0.37% of 3815 structures), has slightly more conformers with inwardly flipped amide C=O groups.

Interestingly, the calculated minimum energy conformation is not perfectly flat for **1c**. Steric repulsion between the quinoline rings is clearly relieved by the compound adopting a nonplanar conformation with its quinoline rings tipped out-of-plane. The energy perturbation required to tip the quinoline rings out-of-plane is, furthermore, surprisingly small. Specifically, only 5.0 kJ/mol is required to drive the torsion angle ϕ_1 for the quinoline ring from 180° to the perpendicular orientation at 90° relative to the central pyridine ring. This suggests (within the limitations of the computational method) that this class of pincer compounds is conformationally considerably more pliant than might be expected at first glance.

Although all the crystallised pincers may populate two main atropisomer conformers, **1c** was the only pincer that crystallised in a chiral Sohncke space group. Compound **1c** thus fits criterion (iii) in Scheme 1, and the remaining pincers fit criterion (iv). These pincers have flexible arms, which enables them to change their conformations through internal degrees of freedom. The barrier governing enantiomerisation determines whether the conformers can interconvert, and therefore directs the

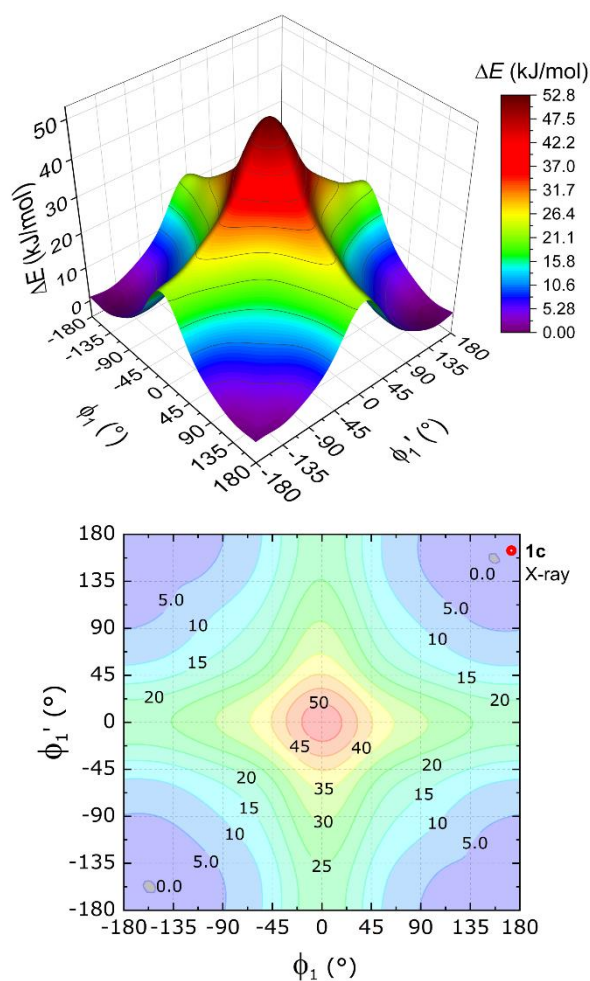


Figure 6. Potential energy surface (3D, top) for **1c** calculated by rotations of ϕ_1 and ϕ_1' (see Figures 4 and 5) in the gas phase using the semi-empirical method PM6. The surface has 2-fold symmetry. The lowest energy barrier to rotation of ϕ_1 (23.11 kJ/mol) occurs at $\phi_2; \phi_1' = 0^\circ; \pm 180^\circ$ (contour map, bottom). The pathway involves the flipping of one amide C=O group while the other substituent maintains coplanarity with the central pyridine ring. The location of the X-ray structure of **1c** is indicated and the global minimum occurs at about $\phi_1; \phi_1' = 150^\circ; 150^\circ$ (mirrored at $-150^\circ; -150^\circ$).

crystallisation of the pincers into chiral (enantiomorphic) or nonchiral (centrosymmetric) Sohncke space groups. It is likely that **1c** becomes locked in one conformer because the distance between its two arms is small, culminating in a substantial barrier of enantiomerisation. The remaining pincers crystallised as racemates as their barriers of enantiomerisation are presumably and by comparison, relatively low.

Racemisation and isomerisation of the present group of pincer compounds is seemingly required to achieve efficient close packing in the crystalline solid state. The principles governing efficient close packing in crystals^{70–72} evidently play a key role in determining the Sohncke space group into which compounds **1a–1f** crystallise. All the current pincer compounds (except **1c**) racemise during crystallization. However, as shown by our analysis of the bulk solids (*vide infra*), racemization is not quantitative and an enantiomeric excess of the M-type atropisomer (left-handed helicity) results in measurable

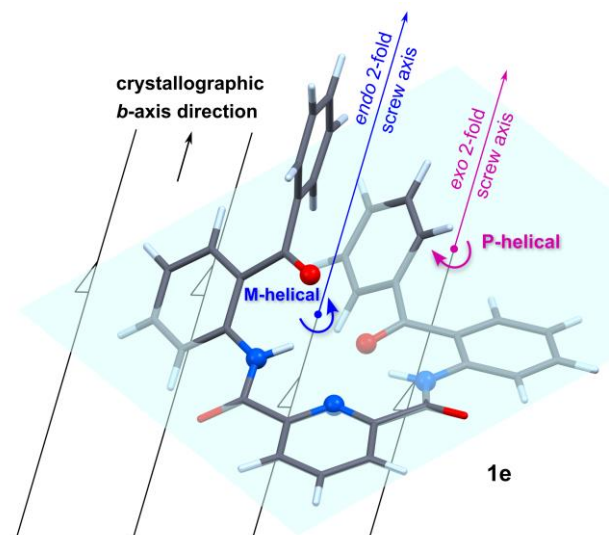


Figure 7. Illustration of the different helicity found at two 2-fold screw axes for crystalline **1e**. The central (intramolecular or “endo”) axis reflects an M-helical conformation (left-handed helicity). Right-handed helicity, i.e., a P-helical conformation, involves the 2-fold screw axis located “exo” to the pincer cavity. The crystal structure in space group $P2_1/n$ has both atropisomer enantiomers (i.e., a racemic mixture) but the M-helicity enantiomer is shown here because an excess population of this enantiomer is observed in solution and the bulk powder solid (see Figure 9). The least-squares plane containing the pyridine ring atoms of the molecule is shown (light blue).

negative intensity CD spectra to a lesser or greater degree (Figure 8).

In addition to the “endo” 2-fold screw axis, and unlike the other pincers, the structure of **1e** has a further two “exo” screw axes involving each of its substituent arms because of the flexibility of the benzophenone groups. Compound **1e** thus has a total of three 2-fold screw (helical) axes, as depicted for the two most-easily visualized axes in Figure 7. Despite having several 2-fold screw axes, the overall conformation of **1e** is determined by its *endo* 2-fold screw axis (i.e., its primary helical axis), which for the structure depicted is a counterclockwise screw (left-handed helicity), thereby assigning the stereoisomer as an M-helicity enantiomer. The P-helicity enantiomer is also present in an exactly equal ratio in the unit cell of **1e** (the single crystal is a racemate). Although the flexible pincer arms of **1e** fit into scenario (iv) of Scheme 1, their exact conformation is influenced by packing interactions with neighbouring molecules, rendering them inflexible in the crystalline solid state and locked in one conformation. For this reason, an excess population of one enantiomer (the M-helical atropisomer) is possible in the bulk powder solid (as show in Figure 9).

CD and UV-vis spectroscopy

Experimental solid-state and solution CD spectroscopic studies of **1a–1f** (Figures 8 and 9) show that all pincers studied exhibited chirality as evidenced by their negative intensity CD spectral peaks. The CD data confirm the presence of an excess population of the M-helicity atropisomer in each sample. For **1c**, this obviously correlates with its X-ray structure and culminates in a strong bulk solid state CD spectrum (Figure 9a). For the remaining compounds, even if racemization has occurred, a

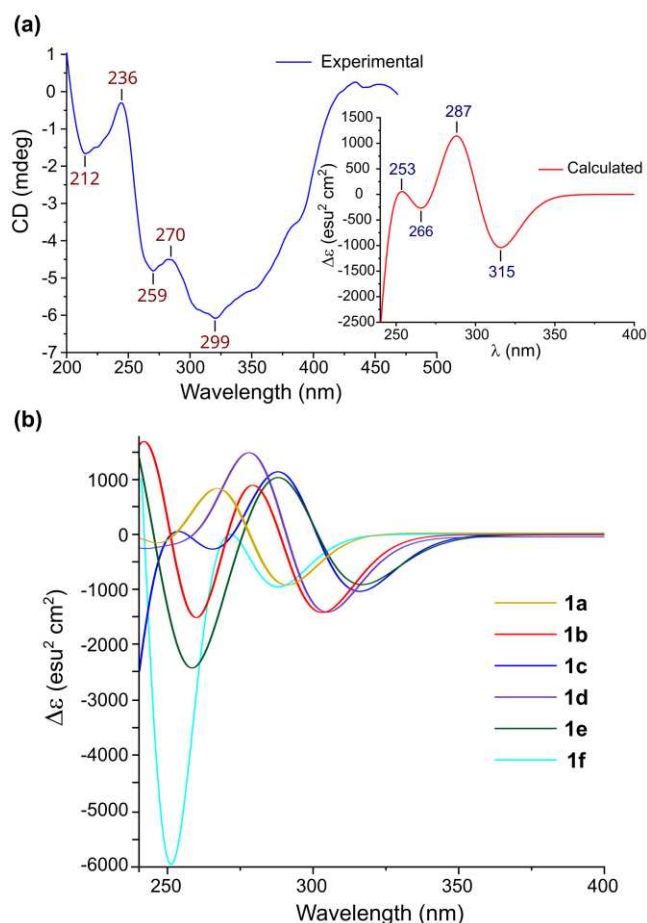


Figure 8. (a) Experimental and DFT-calculated (insert) CD spectra of C_2 symmetry **1c** in chloroform. (b) DFT-calculated CD spectra for **1a–1f** in a chloroform solvent continuum. The calculated spectra were plotted with a full width at half maximum intensity (FWHM) of 3000 cm^{-1} .

slight excess of the M-helicity atropisomer can account for the CD spectra of the bulk solid. The present solid-state CD spectroscopic analysis shows that the M-type atropisomer is the natural state for the pincers and that the CD signals are not spurious. The negative intensity CD spectra were, furthermore, corroborated by TD-DFT simulations in different solvents (Figure 8b) and using a single point calculation on the X-ray structure of **1c**.

The electronic structures of the compounds **1a–1f** were characterised to better understand the electronic structure of the compounds and their CD spectra. The UV-vis absorption spectra of the ligands can be found in the supplementary information. The predicted absorption maxima and the major contributors to each transition are given in Table S1 (supplementary information). Figure 10 showcases the experimental and predicted UV-vis spectra of **1c**, as well as the orbitals and transitions responsible for the major peaks.

Two absorption bands at 310 nm ($\epsilon = 7.4 \times 10^4\text{ M}^{-1}\text{ cm}^{-1}$) and 326 nm ($\epsilon = 8.6 \times 10^4\text{ M}^{-1}\text{ cm}^{-1}$) were observed in chloroform, which correlates with data found in the literature.⁵ Only two peaks (one clear peak and a slight shoulder) were detected when the spectra were recorded in chloroform, as these were the only peaks within the instrument's spectral range. The transitions in chloroform were assigned according to

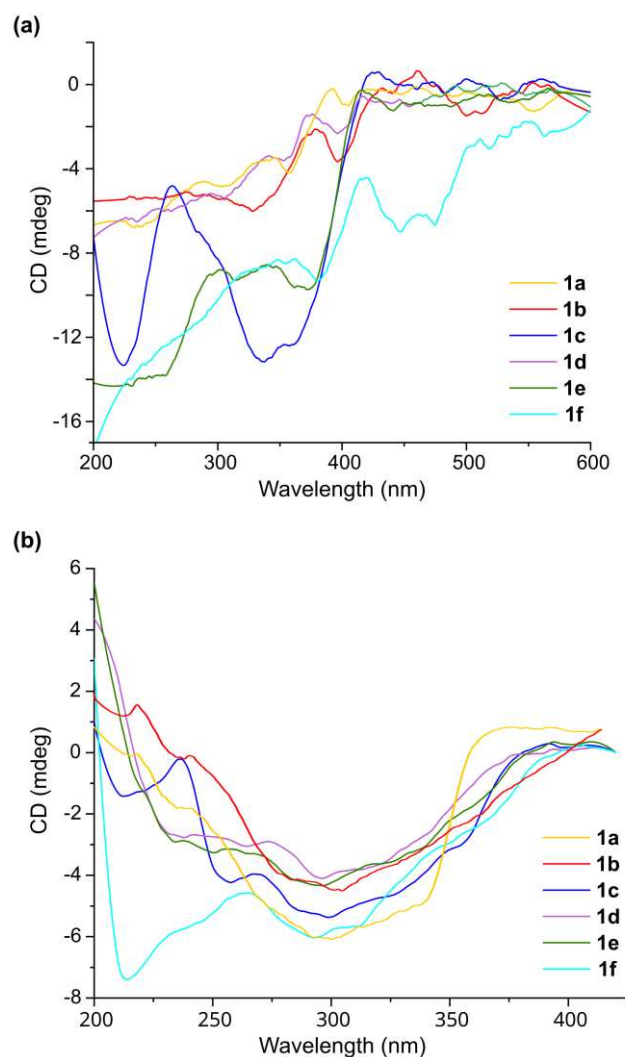


Figure 9. (a) CD spectra for ligands **1a–1f** in the bulk solid state (powder samples for all ligands). The data have been smoothed (250 pt Savitzky–Golay filter). (b) CD spectra for solutions of carboxamide pincers **1a–1b** in 1,2-dimethoxyethane, **1c** in chloroform, **1d–1e** in tetrahydrofuran, and **1f** in methanol. The solvents were selected according to the solubilities of the pincer compounds.

the TD-DFT calculations at the CAM-B3LYP/def2-tzvp level of theory. The DFT-calculated electronic spectrum of **1c** in chloroform is shown in the inset of Figure 10 (a); the broad band centred at 300 nm matches the experimental band well (to within about 25 nm).

Although our experimental CD data showed that the compounds **1a–1f** generally exist in nature and solution as an excess population of one chiral atropisomer (the M-helicity enantiomer), our DFT simulations on **1c** predictably indicated that the two enantiomers have the same energy, confirming that the two stereoisomers are equally stable and that racemization (if feasible via a suitable internal reaction coordinate pathway and unrestricted by the molecule's environment) might be observed.

The frontier molecular orbitals are involved in the low energy transition at 300 nm , as their energy gaps are small. Excitations from HOMO-1 \rightarrow LUMO and HOMO \rightarrow LUMO+1

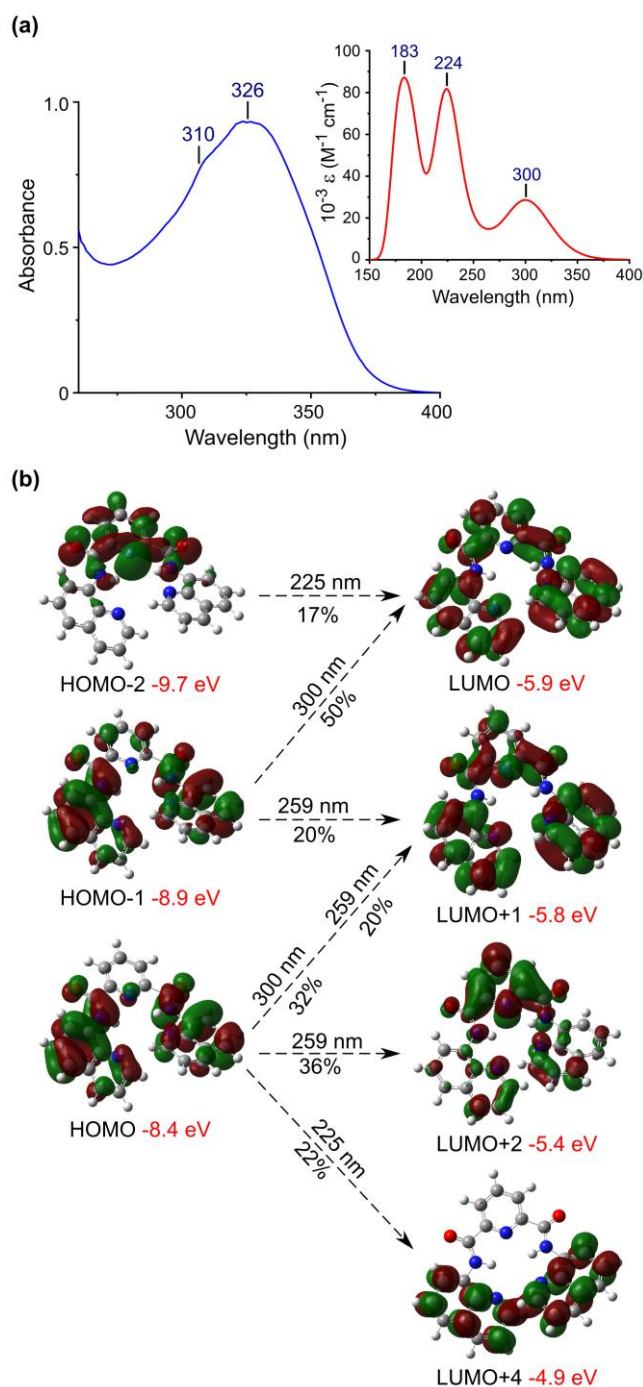


Figure 10. (a) Experimental and DFT-calculated (insert) electronic absorption spectra of C_2 symmetry **1c** in chloroform. The absorption maxima (λ_{max}) are indicated. The absorption envelope for the DFT-calculated spectrum is plotted with full width at half maximum intensity (FWHM) of 3000 cm^{-1} . (b) Molecular orbitals involved in the three most intense bands in the DFT-calculated electronic spectrum of **1c** in chloroform. The percentage contribution of the electronic transitions to each band is indicated.

contribute 50% and 32%, respectively, to the transitions at 300 nm. These are distinctly π - π^* transitions involving π -type MOs centred on the quinoline and pyridine rings.

Variable temperature NMR study of **1d**

Due to the poor solubility of the synthesised compounds, **1d** was selected for variable temperature NMR analysis as a

representative member of the compound group **1a–1f**. Pincer **1d** (5.2 mg) was dissolved in $\text{DMF-}d_7$. NMR spectra were recorded at 10 K intervals from 223–363 K to gather spectroscopic evidence for dynamic conformational changes in the system. In the case of compound **1d**, the existence of atropisomers separated by a relatively large energy barrier can, in principle, enable full or partial chiral resolution of the enantiomers, with the compound becoming largely trapped in one conformer by virtue of intermolecular interactions or another imposed extraneous physical constraint. From Figure 11, it is evident that as the temperature increases from 323 to 343 K, changes in the signal multiplicities for the aromatic protons of **1d** occur along with noticeable line broadening. While the spectral behaviour is not fully commensurate with a typical slow-to-fast exchange equilibrium process for amide rotamers wherein a properly coalesced signal or set of signals is seen between the exchange limits, the data for **1d** at 333 K (broadened, partly coalesced signals) are not fully inconsistent with such a scenario either. Evidently, the temperature-increase within the upper bound of the range studied here allows **1d** to cross one or more barriers, one of which might be the barrier for interconversion between its two symmetry-distinct atropisomers.

To transition between the two atropisomers, molecules of **1d** must pass through a planar geometry where Δ_2 (mentioned in Figure 4 (b) for the related derivative **1c**) is exactly 0° . This rotamer would clearly allow for close interaction between the aromatic protons on the two indazole rings of the pincer arms, thereby perturbing the effective local magnetic field for the aromatic protons. Analysis of the likely transition state for compound **1c** from the PES of Figure 6 suggests that one of the two torsion angles (say ϕ_1) will pass through an angle of 0° while the other stays fixed at 180° . If pincer **1d** behaves similarly and has a similar PES to **1c**, then the transition state structure would favour perturbation of the aromatic proton resonances (notably, the multiplicities and linewidths of the indazole ring protons). The gas phase barrier calculated for **1c** is $\sim 22 \text{ kJ/mol}$. However, a more thorough *ab initio* calculation of the PES for **1d** with inclusion of the solvent would be needed to properly account for the dynamic NMR for this system, a study that falls beyond the scope of the present paper.

Regarding the amide protons of **1d**, Figure 11 indicates that the NH signal broadens (due to enhanced exchange) and exhibits an upfield shift (due to loss of deshielding by an H-bond acceptor). This is consistent with dissociation of H-bonded DMF solvent from **1d** as a function of increasing temperature. The amide NH chemical shift thus correlates linearly ($R^2 = 0.996$) with temperature in the region studied (Figure 11b).

Variable concentration NMR study of **1d**

To evaluate how hydrogen bonding is affected by an increase in concentration, the ^1H NMR spectrum of **1d** was analysed at different concentrations (3.5 – 157 mM) in $\text{DMSO-}d_6$. Self-association by hydrogen bonding with increasing [**1d**] shifts the singlet NH signal downfield with no detectable change in signal multiplicity. The NMR data clearly reflect formation of H-bonded dimers and oligomers akin to the extended X-ray

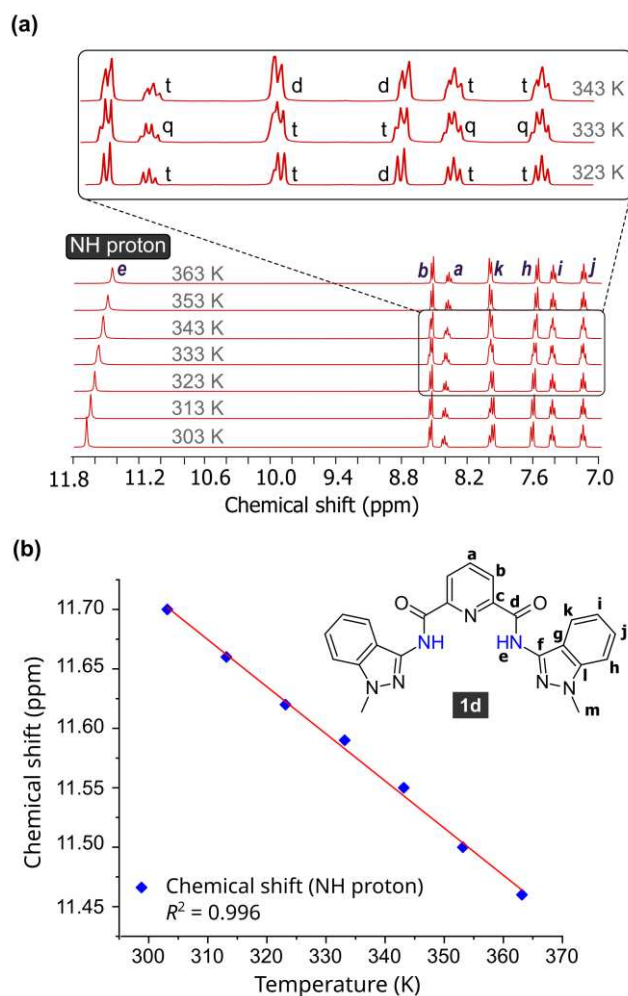


Figure 11. (a) Illustration of the temperature-dependent changes in the ^1H NMR spectrum for **1d** between 303 K and 363 K in deuterated DMF. The inset figure showcases the changes in signal multiplicity (d = doublet, t = triplet and q = quartet) seen for the aromatic protons of compound **1d**. (b) Plot of the amide proton chemical shift as a function of temperature.

structure of **1d** shown in Figure 4. Specifically, the pyridine and indazole protons do not show discernible chemical shift changes with increasing [**1d**] because their magnetic environment(s) remain relatively unchanged. This observation reflects the rather open arrangement (as opposed to a ring-stacked structure) for the H-bonded species seen in the X-ray structure of the compound, and such an arrangement is apparently also favoured in solution. From Figure 12(b), the nonlinear concentration dependence of the NH proton resonance, while subtle, follows a simple polynomial relationship that is commensurate with weak dimer or oligomer formation.^{73,74} The relevant solution equilibrium is depicted by equation 1 below.^{73,74}



Conclusions

A group of related tridentate bis(carboxamide) pincer ligands was investigated. All are C_2 -symmetric chiral compounds, and all have the potential to populate a specific enantiomer under

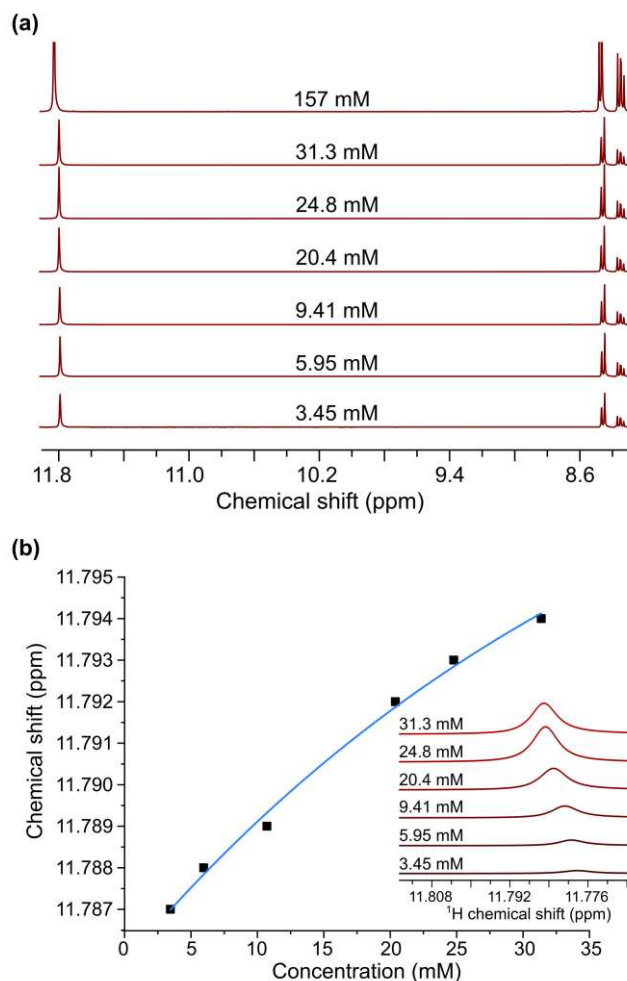


Figure 12. (a) Selected ^1H NMR spectra of the amide proton for **1d** as a function of total concentration in $\text{DMSO}-d_6$ at 25 °C. (b) Simple polynomial fit of the concentration dependence of the amide proton chemical shift. From the nonlinearity of the graph, **1d** likely undergoes weak dimerization in DMSO in accord with the equilibrium depicted in eq. (1).

certain conditions (e.g., limited atropisomerism). Of the five compounds crystallographically characterized here, only the bis(isoquinoline) derivative **1c** crystallised in a chiral Sohncke space group. The steric bulk and intramolecular juxtaposition of the peripheral isoquinoline rings in this system evidently lock in a single, chiral atropisomer in the crystalline solid state. The intrinsic chirality, coupled with the observed stability and flexibility of this group of C_2 -symmetric ligands suggests they might find utility, upon coordination with suitable metal ions, as catalysts suitable for chiral induction in asymmetric synthesis.

Author Contributions

R. R. and O. Q. M. conceived the study. R. R. synthesized and characterized the compounds, performed all spectroscopic measurements, and designed and ran the PM6 and DFT calculations. O. Q. M. performed the crystallography and directed the research. Both authors analysed data, drew figures, and co-wrote the paper.

Conflicts of interest

The authors have no conflicts to declare.

Acknowledgements

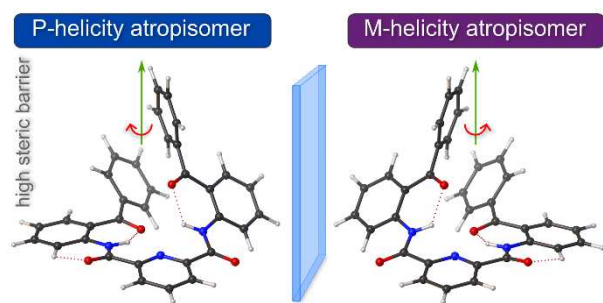
This work is based on research supported by the South African Research Chairs Initiative of the Department of Science and Technology and the National Research Foundation of South Africa (Grant No 64799, OQM). The authors thank WITS University and the NRF for funding to purchase a JASCO J-1500 MCD spectrometer (Grant No 116177, OQM) and the Centre for High Performance Computing (Project CHEM1065, CHPC, Cape Town) for both the CPU time and resources needed for the DFT simulations. The authors thank Dr. Monika Nowakowska for reading a draft manuscript and for her helpful editing comments. We thank a reviewer for suggesting the use of non-spherical atom form factors for the X-ray structure refinements of **1a–1e**.

Notes and references

- 1 A. A. Danopoulos, A. A. D. Tulloch, S. Winston, G. Eastham and M. B. Hursthouse, *Dalton Trans.*, 2003, **0**, 1009–1015.
- 2 C. J. Moulton and B. L. Shaw, *J. Chem. Soc. Dalton Trans.*, 1976, 1020–1024.
- 3 M. A. W. Lawrence, K.-A. Green, P. N. Nelson and S. C. Lorraine, *Polyhedron*, 2018, **143**, 11–27.
- 4 E. Peris and R. H. Crabtree, *Chem. Soc. Rev.*, 2018, **47**, 1959–1968.
- 5 K. Hiratani and K. Taguchi, *Bull. Chem. Soc. Jpn.*, 1990, **63**, 3331–3333.
- 6 W. C. Babcock, R. W. Baker, E. D. Lachapelle and K. L. Smith, *J. Membr. Sci.*, 1980, **7**, 71–87.
- 7 A. M. Costero, M. José Bañuls, M. José Aurell, M. D. Ward and S. Argent, *Tetrahedron*, 2004, **60**, 9471–9478.
- 8 A. Dorazco-González, H. Höpfl, F. Medrano and A. K. Yatsimirsky, *J. Org. Chem.*, 2010, **75**, 2259–2273.
- 9 C. R. Yamnitz, S. Negin, I. A. Carasel, R. K. Winter and G. W. Gokel, *Chem. Commun.*, 2010, **46**, 2838–2840.
- 10 M. Roy, V. Bereznaia, M. Villa, N. Vanthuyne, M. Giorgi, J.-V. Naubron, S. Poyer, V. Monnier, L. Charles, Y. Carissan, D. Hagebaum-Reignier, J. Rodriguez, M. Gingras and Y. Coquerel, *Angew. Chem. Int. Ed.*, 2020, **59**, 3264–3271.
- 11 M. S. Jeletic, C. E. Lower, I. Ghiviriga and A. S. Veige, *Organometallics*, 2011, **30**, 6034–6043.
- 12 K. Choi and A. D. Hamilton, *Coord. Chem. Rev.*, 2003, **240**, 101–110.
- 13 G. Filippini and A. Gavezzotti, *Acta Crystallogr. B*, 1992, **48**, 230–234.
- 14 a_A Miyashita, A. Yasuda, H. Takaya, K. Toriumi, T. Ito, T. Souchi and R. Noyori, *J. Am. Chem. Soc.*, 1980, **102**, 7932–7934.
- 15 S. Grimme and S. D. Peyerimhoff, *Chem. Phys.*, 1996, **204**, 411–417.
- 16 C. Schaack, L. Arrico, E. Sidler, M. Górecki, L. Di Bari and F. Diederich, *Chem. – Eur. J.*, 2019, **25**, 8003–8007.
- 17 S. R. LaPlante, P. J. Edwards, L. D. Fader, A. Jakalian and O. Huckle, *ChemMedChem*, 2011, **6**, 505–513.
- 18 K. M. Clapham, T. Rennison, G. Jones, F. Craven, J. Bardos, B. T. Golding, R. J. Griffin, K. Haggerty, I. R. Hardcastle, P. Thommes, A. Ting and C. Cano, *Org. Biomol. Chem.*, 2012, **10**, 6747–6757.
- 19 R. B. Raffa, J. V. P. Jr and R. T. Jr, *Pharmacol. Pharm.*, 2020, **11**, 1.
- 20 J. W. Jaroszewski, T. Strøm-Hansen and L. L. Hansen, *Chirality*, 1992, **4**, 216–221.
- 21 Q.-L. Zhou, *Privileged chiral ligands and catalysts*, John Wiley & Sons, 2011.
- 22 E. Pidcock, *Chem. Commun.*, 2005, **0**, 3457–3459.
- 23 N. Lavoine, J. Bras, T. Saito and A. Isogai, *J. Polym. Sci. Part Polym. Chem.*, 2017, **55**, 1750–1756.
- 24 N. Lavoine, J. Bras, T. Saito and A. Isogai, *Macromol. Rapid Commun.*, 2016, **37**, 1033–1039.
- 25 P. Kumar, S. Kaur, R. Gupta and K. Bowman-James, in *Pincer Compounds*, ed. D. Morales-Morales, Elsevier, 2018, pp. 295–325.
- 26 D. S. Marlin, M. M. Olmstead and P. K. Mascharak, *Inorg. Chem.*, 2001, **40**, 7003–7008.
- 27 S.-O. Kang, T. S. Johnson, V. W. Day and K. Bowman-James, *Supramol. Chem.*, 2018, **30**, 305–314.
- 28 E. Peris and R. H. Crabtree, *Coord. Chem. Rev.*, 2004, **248**, 2239–2246.
- 29 W. Liu, A. G. Oliver and B. D. Smith, *J. Am. Chem. Soc.*, 2018, **140**, 6810–6813.
- 30 B. Wang, I. G. Howard, J. W. Pope, E. D. Conte and Y. Deng, *Chem. Sci.*, 2019, **10**, 7958–7963.
- 31 H. Wang, J. Liu, Y. Deng, T. Min, G. Yu, X. Wu, Z. Yang and A. Lei, *Chem. – Eur. J.*, 2009, **15**, 1499–1507.
- 32 M. Akaiwa, T. Kanbara, H. Fukumoto and T. Yamamoto, *J. Organomet. Chem.*, 2005, **690**, 4192–4196.
- 33 J. Brooks, Y. Babayan, S. Lamansky, P. I. Djurovich, I. Tsyba, R. Bau and M. E. Thompson, *Inorg. Chem.*, 2002, **41**, 3055–3066.
- 34 F. Neve, A. Crispini, C. Di Pietro and S. Campagna, *Organometallics*, 2002, **21**, 3511–3518.
- 35 T. Kanbara, K. Okada, T. Yamamoto, H. Ogawa and T. Inoue, *J. Organomet. Chem.*, 2004, **689**, 1860–1864.
- 36 E. Heyduk, B. Dummit, Y.-H. Chang and T. Heyduk, *Anal. Chem.*, 2008, **80**, 5152–5159.
- 37 L. Tian, R. E. Wang and Y.-H. Chang, *Antivir Ther*, 2012, **17**, 1437–1442.
- 38 M. Albrecht and G. van Koten, *Angew. Chem. Int. Ed.*, 2001, **40**, 3750–3781.
- 39 B. Bertrand, M. R. M. Williams and M. Bochmann, *Chem. – Eur. J.*, 2018, **24**, 11840–11851.
- 40 G. W. Bates, P. A. Gale and M. E. Light, *Chem. Commun.*, 2007, 2121–2123.
- 41 Q. Yu, T. E. Baroni, L. Liable-Sands, A. L. Rheingold and A. S. Borovik, *Tetrahedron Lett.*, 1998, **39**, 6831–6834.
- 42 M. Rajiv Gandhi, M. Yamada, K. Haga and A. Shibayama, *Sci. Rep.*, 2017, **7**, 8709.
- 43 M. Rajiv Gandhi, M. Yamada, Y. Kondo, A. Shibayama and F. Hamada, *RSC Adv.*, 2016, **6**, 1243–1252.
- 44 O. V. Dolomanov, L. J. Bourhis, R. J. Gildea, J. a. K. Howard and H. Puschmann, *J. Appl. Crystallogr.*, 2009, **42**, 339–341.
- 45 G. M. Sheldrick, *Acta Crystallogr. Sect. Found. Adv.*, 2015, **71**, 3–8.
- 46 G. M. Sheldrick, *Acta Crystallogr. Sect. C Struct. Chem.*, 2015, **71**, 3–8.
- 47 F. Kleemiss, O. V. Dolomanov, M. Bodensteiner, N. Peyerimhoff, L. Midgley, L. J. Bourhis, A. Genoni, L. A. Malaspina, D. Jayatilaka, J. L. Spencer, F. White, B. Grundkötter-Stock, S.

- Steinhauer, D. Lentz, H. Puschmann and S. Grabowsky, *Chem. Sci.*, 2021, **12**, 1675–1692.
- 48 J. W. Furness, A. D. Kaplan, J. Ning, J. P. Perdew and J. Sun, *J. Phys. Chem. Lett.*, 2020, **11**, 8208–8215.
- 49 T. H. Dunning Jr., *J. Chem. Phys.*, 1989, **90**, 1007–1023.
- 50 F. Neese, *Rev Comput Mol Sci*, 2012, **2**, 73–78.
- 51 D. Barnes, R. Chapman, R. Vagg and E. Watton, *J. Chem. Eng. Data*, 1978, **23**, 349–350.
- 52 M. J. Frisch, G. W. Trucks, H. B. Schlegel, G. E. Scuseria, M. A. Robb, J. R. Cheeseman, G. Scalmani, V. Barone, G. A. Petersson, H. Nakatsuji, X. Li, M. Caricato, A. V. Marenich, J. Bloino, B. G. Janesko, R. Gomperts, B. Mennucci, H. P. Hratchian, J. V. Ortiz, A. F. Izmaylov, J. L. Sonnenberg, D. Williams-Young, F. Ding, F. Lipparini, F. Egidi, J. Goings, B. Peng, A. Petrone, T. Henderson, D. Ranasinghe, V. G. Zakrzewski, J. Gao, N. Rega, G. Zheng, W. Liang, M. Hada, M. Ehara, K. Toyota, R. Fukuda, J. Hasegawa, M. Ishida, T. Nakajima, Y. Honda, O. Kitao, H. Nakai, T. Vreven, K. Throssell, J. A. Montgomery Jr., J. E. Peralta, F. Ogliaro, M. J. Bearpark, J. J. Heyd, E. N. Brothers, K. N. Kudin, V. N. Staroverov, T. A. Keith, R. Kobayashi, J. Normand, K. Raghavachari, A. P. Rendell, J. C. Burant, S. S. Iyengar, J. Tomasi, M. Cossi, J. M. Millam, M. Klene, C. Adamo, R. Cammi, J. W. Ochterski, R. L. Martin, K. Morokuma, O. Farkas, J. B. Foresman and D. J. Fox, *Gaussian 16 Revision C.01*, 2016.
- 53 R. Dennington, T. A. Keith and J. M. Millam, *GaussView Version 6*, 2019.
- 54 T. Yanai, D. P. Tew and N. C. Handy, *Chem. Phys. Lett.*, 2004, **393**, 51–57.
- 55 F. Weigend and R. Ahlrichs, *Phys. Chem. Chem. Phys.*, 2005, **7**, 3297–3305.
- 56 R. Bauernschmitt and R. Ahlrichs, *Chem. Phys. Lett.*, 1996, **256**, 454–464.
- 57 G. Scalmani and M. J. Frisch, *J. Chem. Phys.*, 2010, **132**, 114110.
- 58 J. J. P. Stewart, *J. Mol. Model.*, 2007, **13**, 1173–1213.
- 59 Q. Y. Yang, Z. Y. Zhou and J. Y. Qi, *Acta Crystallogr. Sect. E Struct. Rep. Online*, 2001, **57**, o1161–o1162.
- 60 G. W. Bates, P. A. Gale and M. E. Light, *Chem. Commun.*, 2007, 2121–2123.
- 61 Q. Yu, T. E. Baroni, L. Liable-Sands, A. L. Rheingold and A. S. Borovik, *Tetrahedron Lett.*, 1998, **39**, 6831–6834.
- 62 C. R. Groom, I. J. Bruno, M. P. Lightfoot and S. C. Ward, *Acta Crystallogr. Sect. B Struct. Sci. Cryst. Eng. Mater.*, 2016, **72**, 171–179.
- 63 S. Meghdadi, S. Nalchigar and H. R. Khavasi, *Acta Crystallogr. Sect. E Struct. Rep. Online*, 2008, **64**, o431–o431.
- 64 M.-B. Dai, Q.-L. Zhang, X.-C. Zhu, Y. Zhang and B. Zhu, *Chin J Inorg Chem*, 2008, **24**, 1381–1386.
- 65 G. Waris, H. M. Siddiqi, U. Flörke, R. Hussain and M. S. Butt, *Acta Crystallogr. Sect. E Struct. Rep. Online*, 2013, **69**, o416–o416.
- 66 J. Y. Qi, Q. Y. Yang, K. H. Lam, Z. Y. Zhou and A. S. C. Chan, *Acta Crystallogr. Sect. E Struct. Rep. Online*, 2003, **59**, o415–o416.
- 67 R. Kumar, H. Aggarwal, R. Bhowal, D. Chopra and A. Srivastava, *Chem. – Eur. J.*, 2019, **25**, 10756–10762.
- 68 O. Clement, B. M. Rapko and B. P. Hay, *Coord. Chem. Rev.*, 1998, **170**, 203–243.
- 69 S. Akine, S. Sairenji, T. Taniguchi and T. Nabeshima, *J. Am. Chem. Soc.*, 2013, **135**, 12948–12951.
- 70 A. I. Kitaigorodskii, *Acta Crystallogr.*, 1965, **18**, 585–590.
- 71 J. Bernal, K. Knight and I. Cherry, *Nature*, 1964, **202**, 852–854.
- 72 J. B. Goodenough, *Phys. Rev.*, 1953, **89**, 282–294.
- 73 J. S. Chen and R. B. Shirts, *J. Phys. Chem.*, 1985, **89**, 1643–1646.
- 74 O. Q. Munro, S. D. Strydom and C. D. Grimmer, *New J. Chem.*, 2004, **28**, 34–42.

Graphical Abstract



Structural, spectroscopic, and computational studies on C_2 -symmetry bis(carboxamide) pincer ligands indicate excess populations of one atropisomer (enantiomer) are favoured both in solution and the solid state for sufficiently bulky derivatives.